NOAA Technical Memorandum ARL/ATDD-216

AIRBORNE MEASUREMENTS OF MASS, MOMENTUM, AND ENERGY FLUXES, ARCTIC LANDSCAPE FLUX SURVEY (ALFS) - 1994,1995

Steven Brooks
National Research Council Research Associate
Atmospheric Turbulence and Diffusion Division
Oak Ridge, TN

Timothy L. Crawford
Atmospheric Turbulence and Diffusion Division
Oak Ridge, TN

Robert T. McMillen
Atmospheric Turbulence and Diffusion Division
Oak Ridge, TN

Edward Dumas Jr.
Atmospheric Turbulence and Diffusion Division
Oak Ridge, TN

UNITED STATES DEPARTMENT OF COMMERCE

Michael Kantor
Secretary

NATIONAL OCEANIC AND ATMOSPHERIC ADMINISTRATION

D. JAMES BAKER
Under Secretary for Oceans and Atmosphere/Administrator

Environmental Research Laboratories

James L. Rasmussen
Director

NOTICE

Mention of a commercial company or product does not constitute an endorsement by NOAA. Use of information from this publication concerning proprietary products or the test of such products for publicity or advertising purposes is not authorized.

For sale by the National Technical Information Service
5285 Port Royal Road, Springfield, VA 22161

CONTENTS

LIST OF FIGURES

Figure 9a,b Average air temperature (°C) at 10m AGL (A), from the north-south transect, June and August 1995. Daytime data represent all flights occurring between 9am and 9pm Alaskan Daylight Time (ADT). Nighttime data represent those flights between 9pm and 9am ADT. Average surface temperature (°C) (B) from the north-south transect, June and August 1995. Surface temperatures for the mid-August nighttime were not measured due to instrument problems.

Figure 10. Measurements of thawed layer depths made by San Diego State University during the 1994 summer. The three curves represent the thaw depths of a Low Center polygon, an Ice Wedge, and a High Center (HC) Polygon. The aircraft operation periods were in late June (Julian days 170-180), when the average permafrost melting rate was 0.54 cm/day, and mid-August (Julian days 225-235) when the average melting rate was 0.15 cm/day.

Figure 11. Average soil heat flux, G_f (W/m^2) from the north-south transect, June and August 1995. G_f was not directly measured but was calculated by the summation of the net radiation flux, R_f, the sensible heat flux, H_f, and the latent heat flux (water vapor flux), LH_f, ($R_f+H_f+LH_f$).

Figure 12. Average latent heat flux, LE_f (W/m^2) from the north-south transect, June and August 1995. Daytime fluxes show an increasing trend southward. This trend was also observed independently by Eugster *et al.* (1996).

Figure 13. Average sensible heat flux, H_f (W/m^2) from the north-south transect, June and August 1995. A positive flux indicates heat transfer from the surface to the atmosphere.

Figure 14. Average incoming Photosynthetically Active Radiation, PAR (W/m^2), from the north-south transect, June and August 1995. The average nighttime PAR for August was greater than that measured for June. This was due to the short period (3-4 hours) of darkness during the mid-August nights when the aircraft could not be operated because of safety concerns.

Figure 15. Average carbon dioxide flux ($mg(CO_2)\ m^{-2}\ s^{-1}$) from the coastal plain. Data are from the north-south transect during the daytime (9am-9pm, local ADT). Data from June 1994, June 1995, and August 1995 are shown. A negative value indicates that the surface is a sink for atmospheric carbon dioxide

Figure 16. Average carbon dioxide flux (($mg(CO_2)\ m^{-2}\ s^{-1}$) from the coastal plain. Data are from the north-south transect at night (9pm-9am, local ADT).

Figure 17. Average carbon dioxide flux ($mg(CO_2)\ m^{-2}\ s^{-1}$) from the coastal plain. Data are from the east-west transect. The east-west transect was sampled only during the August 1995 daytime hours.

Figure 18. Results from the NOAA ATDD "24 mile" tower from June 24 to July 4. Shown are 30 minute average fluxes (+ source, - sink) and the cumulative carbon dioxide depletion from the surface. The average CO_2 flux shown is 0.029 $mg(CO_2)\ m^{-2}\ s^{-1}$. Gap in the data are periods when the tower was not in operation.

Figure 19. Comparison between tower and aircraft net CO_2 flux estimates made between June 20 and 25, 1995. Aircraft estimates are within $\pm$ 10 latitudinal minutes of the "Happy Valley" tower site.

Figure 20. Expanded average carbon dioxide flux ($mg(CO_2)\ m^{-2}\ s^{-1}$) from the coastal plain. Data are from the north-south transect during the daytime (9am-9pm, local ADT). Data from June 1994, June 1995, and August 1995 are shown. A negative value indicates that the surface is a sink for atmospheric carbon dioxide

LIST OF TABLES

AIRBORNE MEASUREMENTS OF MASS, MOMENTUM, AND ENERGY FLUXES, ARCTIC LANDSCAPE FLUX SURVEY (ALFS) - 1994,1995

Steven Brooks, Timothy Crawford, Robert McMillen and Edward Dumas

National Oceanic and Atmospheric Administration (NOAA) Atmospheric Turbulence and Diffusion Division (ATDD), 456 S. Illinois Avenue, P.O. Box 2456, Oak Ridge, TN 37831

ABSTRACT. During the summer months of 1994 and 1995, NOAA's Atmospheric Turbulence and Diffusion Division, in conjunction with San Diego State University, measured flux densities of mass (CO_2 and H_2O), momentum, and energy from a tower (1994) and an airplane (1994,1995). The aircraft was flown along one latitudinal and one longitudinal transect on the North Slope of Alaska. The experiment consisted of two weeks of continuous tower measurements and over 100 aircraft flights, occurring over a range of weather conditions during both daytime and evening hours. The majority of the flights (approx. 90%) were along the fixed N/S or E/W transects, while the remainder were profile patterns to determine boundary layer characteristics.

As part of the National Science Foundation (NSF) Arctic System Sciences (ARCSS) Land-Atmosphere-Ice Interaction (LAII) flux program, the goal of the Arctic Landscape Flux Survey (ALFS) was to estimate the diurnal and seasonal landscape, and regional flux patterns, to develop methods of scaling between these spatial and functional scales for extrapolation to other circumpolar tundra regions, and to develop predictive capabilities for estimating the potential effects of global climate change on the arctic tundra ecosystem.

This report describes the variations in radiation and surface temperature, along with exchange of mass, momentum, and energy observed at the tower site and along the aircraft transects.

1. INTRODUCTION

High-latitude warming has been recently reported in arctic Alaska, Canada and Russia. Thermal profiles of permafrost indicate a temperature rise of 2-4°C across the north slope of Alaska and throughout northern Canada within the last century, or possibly even during the last few decades (Lachenbruch and Marshall, 1986; Beltrami and Mareschal, 1991). Near Barrow, Alaska, surface temperature has increased by approximately 1.5°C over the 80 year average during the last decade alone (Oechel et al., 1993).

Northern high-latitude ecosystems are particularly vulnerable to climate change due to the large carbon stocks in northern latitude soils and the predominance of permafrost. Northern ecosystems (arctic, boreal forest and northern bogs) represent approximately 14% of the total global land area, however, they contain approximately 25% of the total global soil carbon pool in the permafrost and seasonally thawed soil active layer (Miller et al., 1983). Tundra ecosystems have historically sequestered carbon and alone contain approximately 180 Pg, or 12% of the global soil carbon pool, even though they only make up about 6% of the total land area (Miller et al.,1983). A comprehensive study of the Alaskan arctic tundra environment is intended to provide one piece of the global carbon balance puzzle.

San Diego State University researchers began limited Alaskan north slope CO_2 flux measurements in 1983 with closed greenhouse chambers. Over the next 11 years the program grew to encompass larger areas of the north slope and to include tower-based measurements. These initial study years indicated that the north slope tundra was a source of CO_2 to the atmosphere at a rate of 53 to 286 g C m^{-2} yr^{-1} (Oechel et al., 1993). In light of these results the program was expanded to include the National Oceanic and Atmospheric Administration Atmospheric Turbulence and Diffusion Division (NOAA/ATDD) flux measurement capabilities. The NOAA/ATDD efforts during 1994 and 1995 included aircraft and tower based measurements. This expansion from the plot to the regional and landscape scales helps to determine the effect of climate change on arctic ecosystems, and potential positive and negative feedback of arctic ecosystems on regional and perhaps global climate.

This study highlights the use of towers and light aircraft to conduct season-long measurements of surface/atmosphere fluxes, spectral indices and meteorological and near-surface variables for global change research. The program was built on a successful collaboration between San Diego State University and the NOAA/ATDD scientists over the last several years. It also contributes to a comprehensive ecosystem and global change research program in the arctic.

2. ALASKAN NORTH SLOPE COASTAL PLAIN ENVIRONMENT

The study area consists of a gently sloping plain from the foothills of the Brooks Range to the Beaufort Sea. The three major rivers are: the Sagavanirktok, the Colville, and the smaller Kuparuk. Additional small streams are very common throughout the area. The majority of the rivers and streams flow directly from south to north. The tundra of the coastal plain is classified as moist/wet non-acidic (Walker, 1996). This study area is important as the moist/wet non-acidic is a predominate tundra type throughout the circumpolar arctic.

The summertime coastal plain contains large amounts of standing or slow moving water as drainage is impeded by a underlying continuous permafrost layer. Permafrost, in general,

is located in regions where the average temperature is less than -6°C. The depth of the seasonally thawed layer is controlled by seasonal fluctuation of surface temperature about the mean (Gold and Lachenbruch, 1973; Lachenbruch, 1968). The very gentle sloping of the coastal plain and the shallow nature of the thawed layer and gravel bed rivers means that movement of water throughout the coastal plain is very slow. Tracers added to water-logged soils within the center of the coastal plain (40km from shore) were detected in river water one year later (Kane et al., 1996).

Mean annual temperatures range between -12.8 and -10.3°C (Oechel and Billings, 1992), while the mean summer temperature (June-August) is near +4°C. Precipitation ranges between 180-210 mm, with the majority falling as snow during the fall-spring months (Kane et al., 1996). Because of the seasonally cold temperatures, snowmelt typically occurs during June (Kane et al., 1996) and the growing season, late June to early September, is significantly shorter than in the interior regions of Alaska (Oechel and Billings, 1992).

The surface of the coastal plain tundra consists mostly of mosses and grasses with a living biomass density of $\approx$500 g/m^2 and a maximum vegetation height of $\approx$25 cm (Shaver, 1996). Larger shrubs dominate near river beds in the southern portion of the study region. The primary limit on plant production is lack of available nitrogen (Shaver, 1996). Plant production in turn effects the size and growth rates of the summertime migratory grazers, mainly Caribou herds and Geese flocks.

On tundra, atmospheric carbon dioxide is taken up by plant Photosynthesis (P) and released in Respiration (R) and Aerobic Decomposition (AD). The net CO_2 flux to the atmosphere is the difference between these competing quantities, R+D-P. Methane, CH_4, is diffused into the atmosphere from soil AnAerobic Decay (AAD) and to a smaller degree is removed from the atmosphere by Oxidation (O) at soil surfaces. The net flux of methane to the atmosphere is therefore AAD-O.

A schematic of the coastal plain tundra carbon balance is shown in Fig. 1. Ground waters on the coastal plain contain CO_2, CH_4 and Dissolved Organic Carbon (DOC). Open waters, such as rivers and lakes, release CO_2 and CH_4 to the atmosphere. In lakes, dissolved organic carbon breaks down releasing additional methane to the atmosphere. From measurement of partial pressures of CO_2 and CH_4 Hobbie (1996) has concluded that all waters in the alaskan arctic tundra are sources of CO_2 and CH_4 to the atmosphere. This report focuses only on the CO_2 fluxes.

Summertime coastal plain tundra soil typically consists of a dry or moist top layer, 0-20 cm deep over a water logged soil layer of 10-40 cm. Continuous underlying permafrost traps snow melt and rain water in the near surface soil. The upper portion of the soil consists of an organic layer 15-30 cm in depth. The summertime active layer depth (depth of the seasonal thawed layer) varies between 0 and 60 cm (Ping, 1996) with the maximum occurring in September. Overall, the top one meter contains $\approx$62 kg(C)/m^3 with an average carbon age of roughly 4,000 years (Ping, 1996).

ARCTIC CARBON BALANCE

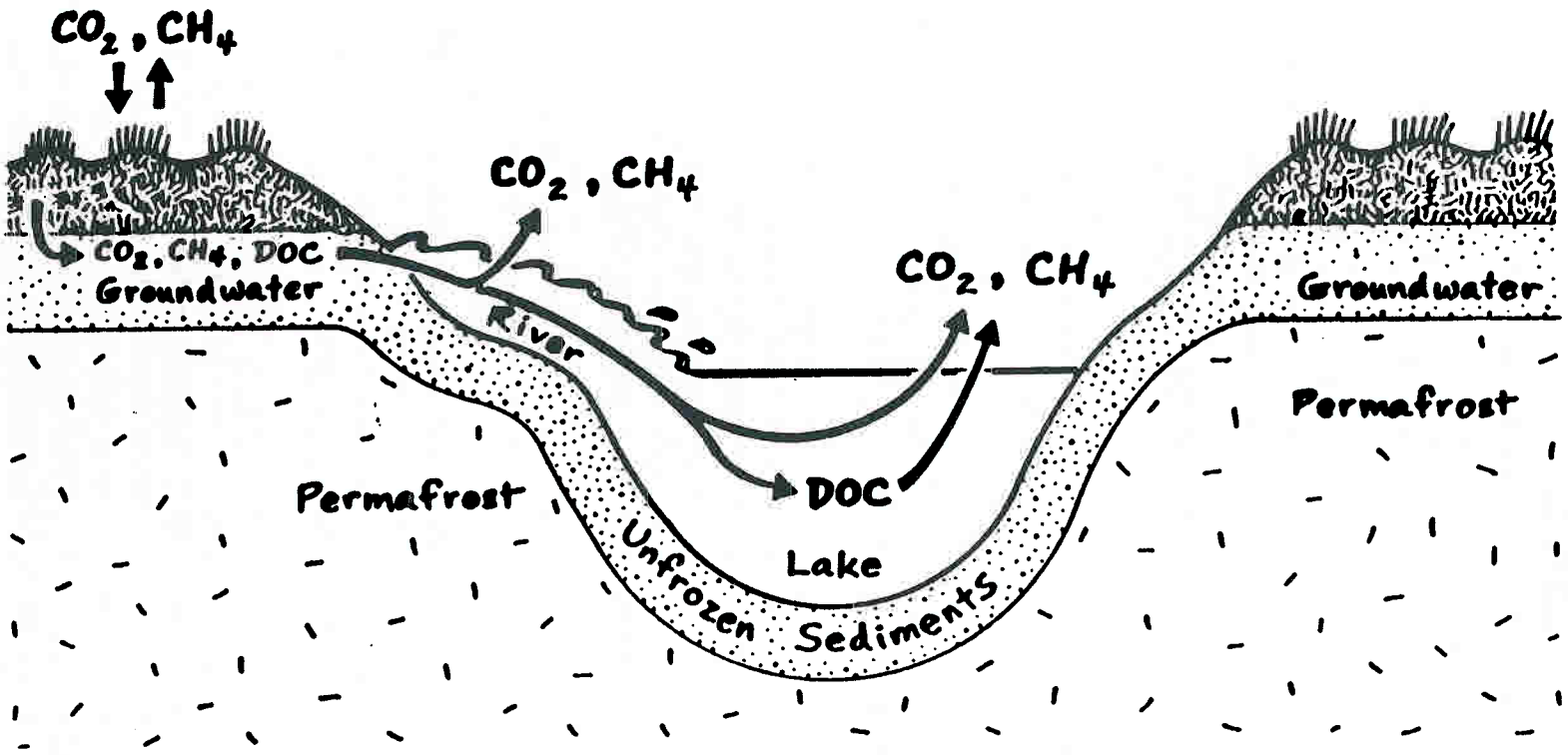

Figure 1. A schematic of the coastal plain tundra carbon balance. Ground waters on the coastal plain contain CO_2, CH_4 and Dissolved Organic Carbon (DOC). Open waters, such as rivers and lakes, release CO_2, CH_4 to the atmosphere. In lakes dissolved organic carbon breaks down and additional methane is released to the atmosphere.

The active layer depth determines the quantity of available nitrogen and carbon for plant, microbe/fungi decomposition, and the soil moisture by the melting of the seasonally frozen layer and the pooling of water near the surface (Flanagan and Bunnell, 1980; Chapin, 1983; Hinzman and Kane, 1992). In turn the seasonally thawed depth is dependent on vegetation, solar radiation, and temperature. A relationship model of the near surface tundra environment is shown in Fig. 2.

3. THE ARCTIC LANDSCAPE FLUX SURVEY (ALFS) EXPERIMENT

Micrometeorological techniques have proven to be useful in the characterization of landscape level fluxes of CO_2, H_2O vapor, and energy balance (Baldocchi et al., 1988). Using tower and aircraft platforms, eddy correlation techniques allow the quantification of material fluxes on hectare and square kilometer scales (Baldocchi et al., 1988; Desjardins et al., 1989), respectively. Eddy correlation methodology was used during the Arctic Boundary Layer Expedition, ABLE-3, campaign to quantify short-term CO_2 and CH_4 fluxes in Alaskan sub-arctic tundra (Fan et al., 1992). Although measurements were made only during the season peak (mid-July to mid-August), landscape-level estimates of CO_2 and CH_4 flux are comparable to plot scale measurements (Fan et al., 1992). Eddy correlation methods also appear to be sensitive to landscape level variations in soil moisture and vegetation type, thus allowing the determination of large scale controls on material and energy fluxes (Fan et al., 1992).

The ALFS experiment base of operations was located in Deadhorse, which presented the only paved runway in NE Alaska. From Deadhorse, daily flights consisted of a beginning profile pattern followed by repeated transect flights, and ended with a profile pattern. The transect flights were flown at 10 to 15 m Above Ground Level (AGL). These flights provided measurements of surface flux behavior. The profile patterns, from the surface to 500-2000 m, provided temperature, moisture and wind speed profiles through the atmospheric boundary layer.

The main transects were a 100 km north-south transect between Deadhorse and Slope Mountain, Alaska (70°12' 148°55', 69°24' 148°55') flown during late June of 1994 and late June and mid-August of 1995, and a 100 km east-west transect (69°54' 148°00', 69°54' 152°00') flown during mid-August of 1995. The transects and a map of northeast Alaska are shown in Figure 3. The tower sites shown in Fig. 3 were tower based eddy correlation flux measurement sites maintained by San Diego State University during the summer months of 1994 and 1995. The combination of continuous tower flux measurements and spatial aircraft measurements is an effective tool for large area flux estimations.

4. THEORY OF EDDY FLUX MEASUREMENTS

Air/surface exchange, or the surface flux, is a fundamental boundary condition controlling the atmospheric boundary layer and its mass, momentum, and energy budgets. The

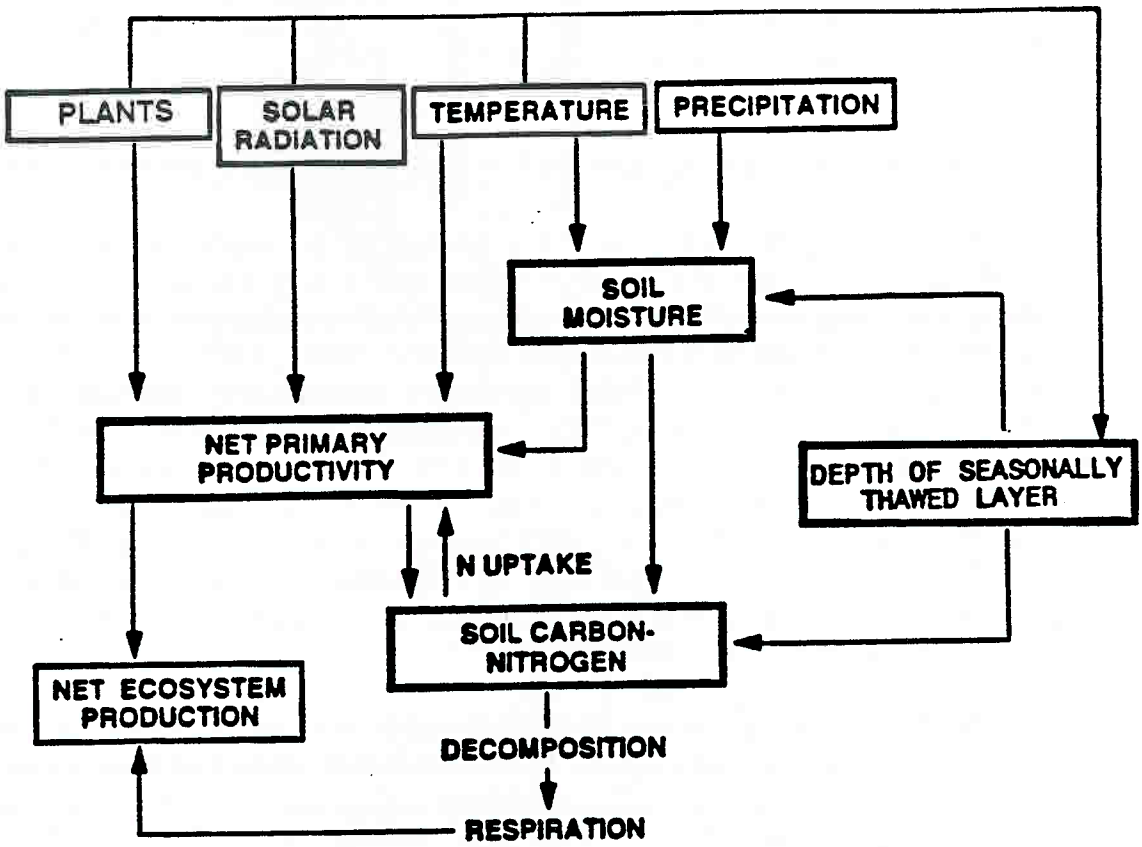

Figure 2. A possible relationship model for the tundra near surface environment.

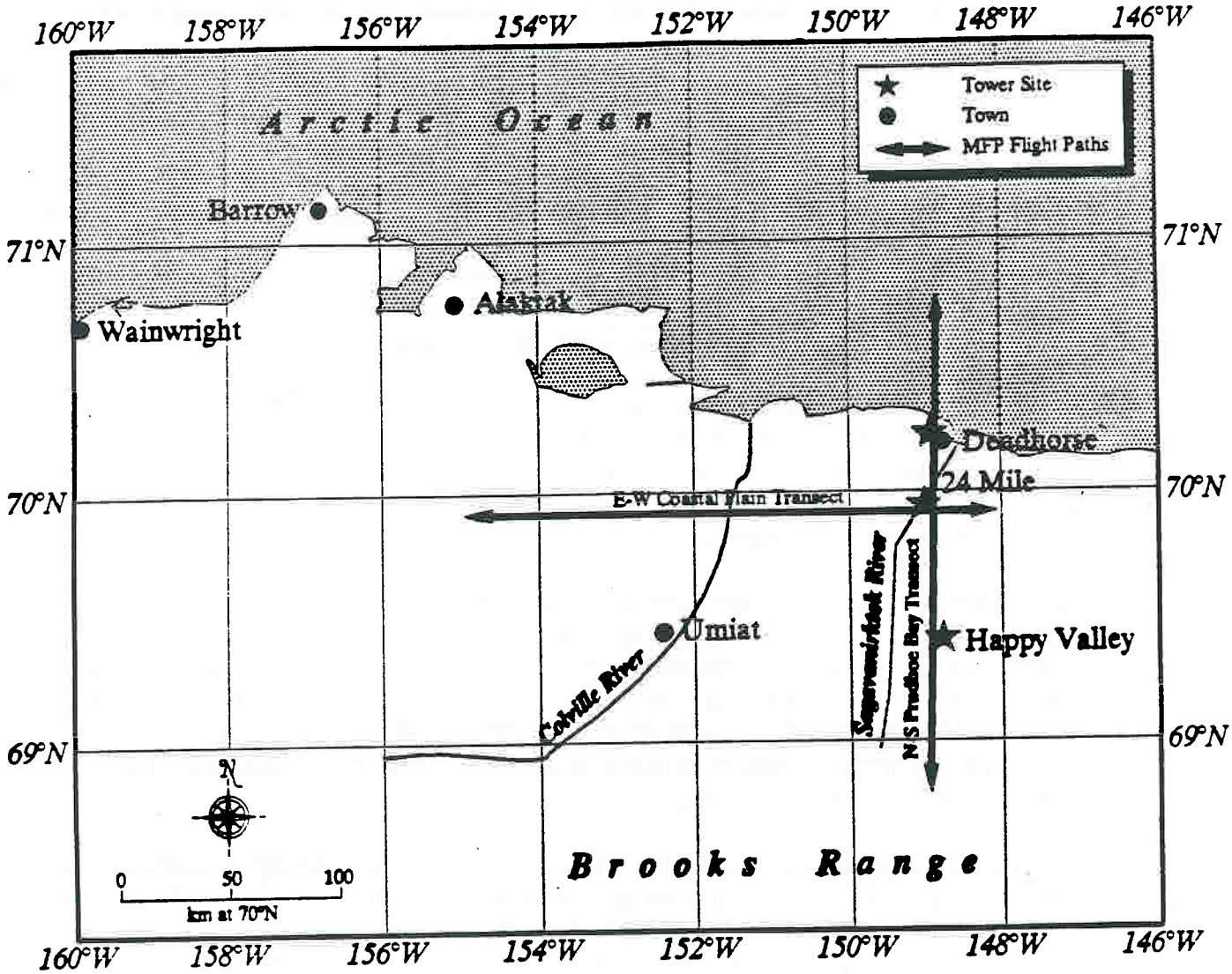

Figure 3. Map of a portion of the Alaskan north slope. Shown are the aircraft north-south and east-west transects along with major rivers, tower sites (stars) and towns (circles). Flight operations were conducted out of Deadhorse.

quantity exchanged at the surface passes through the near surface boundary layer by turbulent transport. Thus, the surface exchange may be determined by measuring the near-surface turbulent or "eddy" flux. The eddy flux is simple in concept, mathematically expressed as the covariance

$$F = \langle (rw)'s' \rangle . \qquad 1$$

Here (rw)' is the vertical turbulent fluctuation of the product of the dry air density and vertical velocity (i.e. dry air mass flux density), and s' is the turbulent fluctuation in the mixing ratio, relative to dry air, of the species of interest. The angle brackets indicate the appropriate ensemble average.

The desirability of the method derives from its direct nature, first principles basis, noninvasive nature and short time scale. Since the near-surface flux is directly observed, the only assumption is that the flux divergence or gradient between the measurement and the surface is small. This assumption is valid when other terms such as mean transport, source, and storage within the conservation equation are small. The reliability of this assumption weakens with increasing measurement altitude and increasing complexity in atmospheric and surface conditions.

The measurement principles for wind velocity and species concentration are well developed. Since the flux measurement is made above the surface without disturbing the surface itself, it cannot influence the exchange observed. Tower observations using a 15-min time scale, and airborne observations using a 3 km space scale, give data with sufficiently small time/space scale to permit the process studies needed to improve predictive capabilities. In the last ten years, the accuracy of this technique has improved because of significant advancements in instrumentation and processing techniques.

However, the details associated with proper instrument operation, data processing and data interpretation are complex. This is especially true for airborne flux systems. For aircraft, both the instrument systems and data processing programs are an order of magnitude more complex when compared to tower systems. For example, on an aircraft, one must observe the air-velocity relative to the sensors and then subtract from this the sensor velocity relative to earth. Both vectors are large and only the small difference, the vector wind with respect to earth, is of interest. Neither vector can be directly observed, but must be synthesized from numerous sensors. The synthesis process is intolerant of phase or amplitude errors introduced by sensors, data systems or processing algorithms.

From the NOAA ATDD aircraft system, fluxes are usually measured approximately 10m above the surface (higher from other aircraft and lower from towers). The flux measurement accurately defines the flux occurring at the flight altitude and along the flight track. However, the purposes of this study was to measure the surface flux. The flux observed at flight altitude is representative of the surface flux if the following conditions are met.

1. The flight altitude is low enough to be within the constant flux layer. Above this, flux divergence becomes increasingly more important with increasing altitude where the observed flux is no longer representative of the surface flux. Such flux divergence usually causes an underestimation of the surface flux, but not always. Typically, mitigating flux divergence concerns requires measurement altitudes to be within the lower 10% of the turbulent boundary layer. The Long-EZ's 10m sampling altitude satisfies this requirement.

2. The underlying surface is homogeneous. It should extend upwind of the flight track for about 100 times the sampling altitude. Also, it should extend along the flight track for a distance equivalent to the space average being applied in data processing. This ensures the development of an equilibrium surface boundary layer and adequate sampling time before conditions change. The physical measurements made from the airplane remain valid whether or not these conditions are met. However, small-scale inhomogeneity greatly increases the difficulty of specifying and interpreting the mean state from which the turbulence departs and introduces samples from multiple populations into the measurement set.

3. Stationary meteorological conditions prevail during sampling. Such conditions as frontal passage and nightfall clearly violate this, featuring important contributions from horizontal transport or storage terms, explicitly rejected by Eqn. 1. However, less abrupt changes can also be important. For example, if the air temperature is warming 3 deg/hr, the heat flux at 15 meters will be 20 W/m^2 less than at the surface due to thermal storage.

5. MOBILE FLUX PLATFORM

The NOAA ATDD Mobile Flux Platform (MFP) is a cluster of collocated instruments whose data are simultaneously logged by a single computer system. The MFP system can be mounted on a variety of vehicles (aircraft, boats, etc.) and is primarily used to measure atmospheric turbulent structure and trace-gas air-surface exchange. The development of the MFP system responded to research needs for a low cost system capable of measuring representativeness and spatial variability of air-surface exchange in various environments.

For this experiment a variant of the Rutan "Long-EZ", a two passenger high-performance airplane, was selected to carry the MFP. Aerodynamic characteristics of the Long-EZ are well suited for long-duration, high-fidelity turbulent flux measurements. The "pusher" configuration leaves the front of the airframe free of propeller-induced disturbance, engine vibration, and exhaust. The small, light-weight, laminar-flow airframe has an equivalent flat plate drag area of only 0.2 m^2. The nose region thus has minimal flow disturbance, and is ideal for measurement of winds, temperature, and trace species using the unique turbulence

probe developed at ATDD (Crawford and Dobosy, 1992). The canard design has a low stall speed with no spin hazard. The plane has superior pitch stability in turbulent conditions. These factors, combined with low wing loading, allow safe, low-speed (50 ms^{-1}), and low-level (10 to 20 m AGL) turbulence measurements within the boundary layer, which has been a difficult venture for instrumented aircraft in the past (Table 1).

Table 1. Meteorological and turbulence parameters measured with the MFP equipped Long-EZ.

METEOROLOGICAL STATE PARAMETERS	TURBULENT FLUXES
Winds (U, V, W) Position (X, Y, Z, t) Temperature, Dew Point Pressure H_2O, CO_2 Radiation, Surface Temp.	Momentum Sensible Heat Latent Heat CO_2

Table 2 lists the Long-EZ aircraft's specifications and performance characteristics. The airplane is IFR-equipped (including weather radar), and has a ceiling exceeding 9 km AMSL. The airframe is of fiber composite construction, conforming to the +9 to -6 G-load requirements of the acrobatic class airframe. This fatigue-resistant and high-strength characteristic provides safe operation even in high levels of thermal or mechanical turbulence. To enhance flight safety, a ballistically-deployed parachute system, opening in 0.9 s, allows emergency recovery of the pilot, airplane, and instrumentation. The long range capability of the Long-EZ allows easy access to sites such as the North Slope.

Table 2. Long-EZ airplane specifications.

Specifications		Performance	
Type Certificate	Experimental	Stalling Speed	27 ms^{-1}
Powerplant	Lyc-O-320 160 HP	Maximum Speed	93 ms^{-1}
Electrical	65 amp 12VDC	Ceiling	9000 m
Empty Weight	430 kg (950 lb)	Range	3300 km
Gross Weight	725 kg (1,600 lb)	Endurance	10 to 18 hr
Fuel Capacity	200 kg (435 lb)	Fuel Use	8.2 to 19 $kg\text{-}hr^{-1}$
Wing Area	9.3 m^2	Flow Blockage	0.2 m^2

An understanding of the equipment used onboard the MFP is not complete without an understanding of the eddy correlation technique of surface flux measurements. An

appropriate discussion on that topic is provided in the next section. Details about the in-flight and post-flight processing of meteorological state parameters, together with details on the flux calculation algorithms follow.

6. EDDY FLUX MEASUREMENT TECHNIQUE

A significant part of the complexity of this measurement lies in separating turbulent fluctuation from mean and defining an appropriate ensemble average. Equation 1 is not computationally useful until the turbulent fluctuations are defined. Traditionally, the fluctuations are defined as

$$s = s' + S \qquad 2$$

where S is the appropriate ensemble mean of s. Given this definition, Eqn. 1 may be rewritten as

$$F = \langle (rw - RW)(s - S) \rangle \qquad 3$$

Here, RW is not the mean of the dry air density times the mean of the vertical velocity but is the mean of the product. For heat flux, $s = C_p{}^*T$ where C_p is the moist air specific heat at constant pressure. C_p depends locally (i.e. at 40 Hz) on water vapor concentration. T is the potential temperature. The use of potential temperature compensates for the compressible nature of the atmosphere. For latent heat flux, $s = Lq$ where L is the local temperature dependent evaporation energy for water, and q is the water vapor mixing ratio relative to dry air. For CO_2, s becomes the CO_2 mixing ratio relative to the dry air component. This approach satisfies the constraint outlined by Webb et.al. (1980) that there be no flux of dry air and implicitly corrects all fluxes for heat and water vapor transport.

On a tower, the mean is defined as a time average. The fluctuation is then obtained as $s' = s - S$ where S is the average over time periods of approximately 15 to 30 minutes. From aircraft, however, s observed contains both space and time related trends. In aircraft flux data, space trend should also be considered.

Eddies in a wide range of scales contribute to turbulent transfer. Successful eddy flux measurement requires proper sampling over this spectrum. The eddy-size is expressed by a dimensionless frequency, nz/u, where n is the eddy-size as a frequency, z the sampling height and u the eddy transport speed past the sensor. The important eddy-size range contributing to turbulent transfer is typically $0.005 < nz/u < 5$. For the Long-EZ, u = 50 m/s and z = 10 m. Therefore, from the Long-EZ, eddy-size between 1.25m and 1.25km are important. The nz/u scaling points out the need for and advantage of fast turbulent systems. Fast sensors/data enhance the spatial resolution of the flux observation.

Evaluating the accuracy of the eddy correlation method is not straight forward. Factors contributing uncertainties include: instrument errors, sensor time response, signal to noise

ratio, sensor separation distance, height of the measurement, and signal attenuation due to path averaging and sampling through tubes. Natural variability due to non-steady conditions, turbulence intermittency, and surface inhomogeneities, adds additional uncertainty.

7. VELOCITY AND TEMPERATURE MEASUREMENTS

Three-dimensional wind component and temperature measurements were obtained with a sensitive, fast-response turbulence probe (Crawford and Dobosy, 1992). The velocity vector at the probe is obtained by adding the velocity $\mathbf{V}_a$ of the air relative to the probe to the velocity $\mathbf{V}_s$ of the probe. This gives the velocity $\mathbf{V}$ relative to earth:

$$\mathbf{V} = \mathbf{V}_s + \mathbf{V}_a. \qquad 4$$

The algorithm used to determine the probe velocity vector ($\mathbf{V}_s$) uses input from accelerometers to obtain high frequency contributions (Crawford *et al.* 1990). Input from a Global Positioning System (GPS, Dobosy et al., 1996; Crawford and Dobosy, 1992) was used to obtain low frequency contributions. The velocity vector relative to the probe ($\mathbf{V}_a$) is computed from pressure differences observed on the probe. The probe is unique in that it collocates the sensors (acceleration, pressure and temperature) needed for accurate high frequency measurements of wind and temperature. The probe is mounted axi-symmetrically on the airplane. Many sensors used in the algorithm for air motion computation are summarized in Crawford *et al.* (1990) and Dobosy *et al.* (1996).

8. IN-FLIGHT DATA PROCESSING

Fast and slow response analog signal data were first conditioned with 30 Hz low-pass, anti-aliasing, five-pole Butterworth filters before being converted to 200 Hz digital signals. The 200 Hz fast response digital signal was passed through a five-point Hanning filter, subsampled at 40 Hz, and written to disk for post processing. Slow response analog signal data were also digitized at 200 Hz, but were passed through a two stage digital filter before being subsampled at 1 Hz for recording. The first stage was a five-point centered average, subsampled at 40 Hz. The second stage was a 40 point triangle filter rejecting frequencies above 1 Hz.

9. POST-FLIGHT DATA PROCESSING

Upon returning from the experiment, all sensors were recalibrated with ATDD lab standards. The final calibration used in data reduction was based on analysis of pre-field, field, and post-field instrument response checks and daily pre-flight and post-flight multipoint calibrations. The next step was a run-by-run quality acceptance (QA). The QA checks consist of displaying time series and checking the mean, standard deviation, maximum, minimum, skewness and kurtosis for each run. Following this winds are computed by Eqn. 4.

Path average heat, momentum, water vapor, and CO_2 fluxes are computed during post processing using Eqn. 3 which implicitly removes the means (but not trends). As outlined by Webb *et al.* (1980), necessary data corrections for pressure, temperature, and water vapor fluctuations were eliminated by converting sensor outputs to mixing ratios (*i.e.* the species mass density divided by the mass of dry air) as required by Eqn. 1.

10. SUMMERTIME ATMOSPHERIC BOUNDARY LAYER OVER THE TUNDRA

The vertical profiles of the atmospheric boundary layers were periodically measured as part of each field study. The measured boundary layer heights are shown in Fig. 4. The atmospheric boundary layers are divided into stable and convective types. The transitions from convective to stable and stable to convective occur roughly at 1830 and 0900 Alaskan Daylight Time (ADT), respectively.

Stable boundary layers over the arctic tundra in the summer evenings are formed as winds blow over cooler terrain where the roughness scales are small. The turbulence is generated only by shear at the surface and is damped by the stable overlying air mass, so that turbulence energy decreases rapidly with height (Dabberdt *et al.*, 1993). This results in stable very thin boundary layers ($\approx$100m) with very little vertical mixing except very close to the surface (<10-20m).

During the stronger sunlight periods, a convective boundary layer is formed. This forms as the surface is heated by the summer sun and the air at the surface becomes convectively unstable. This results in thicker boundary layers ($\approx$500m) with enhanced vertical mixing (Dabberdt *et al.*, 1993).

Profiles of water vapor, air temperature, and potential air temperature are shown in Figs. 5a,b,c and 6a,b,c for nighttime stable and daytime convective boundary layers respectively. These measurements were made as the aircraft flew profile patterns. The approximate latitudes of the ascending and descending portions of the profiles are shown in the figures.

Figures 5a,b,c are inland boundary layer profiles measured over the coastal plain during clear weather and light winds from the North on July 1, 1994 at 0930 GMT (1:30 am Alaskan Daylight Time, ADT) along the North-South transect (Long. = 148.9°). The profiles indicate that the air near the ground was extremely stable due to temperature increase with height. The boundary layer was extremely thin ($\approx$230m) with rapid vertical mixing only in the lowest 100-150m as indicated by the correlation of potential temperature and water vapor concentrations. Uniform horizontal mixing, a characteristic of shear generated boundary layers (Stull, 1988), is indicated by the similarity of the water vapor profiles measured $\approx$12 km apart.

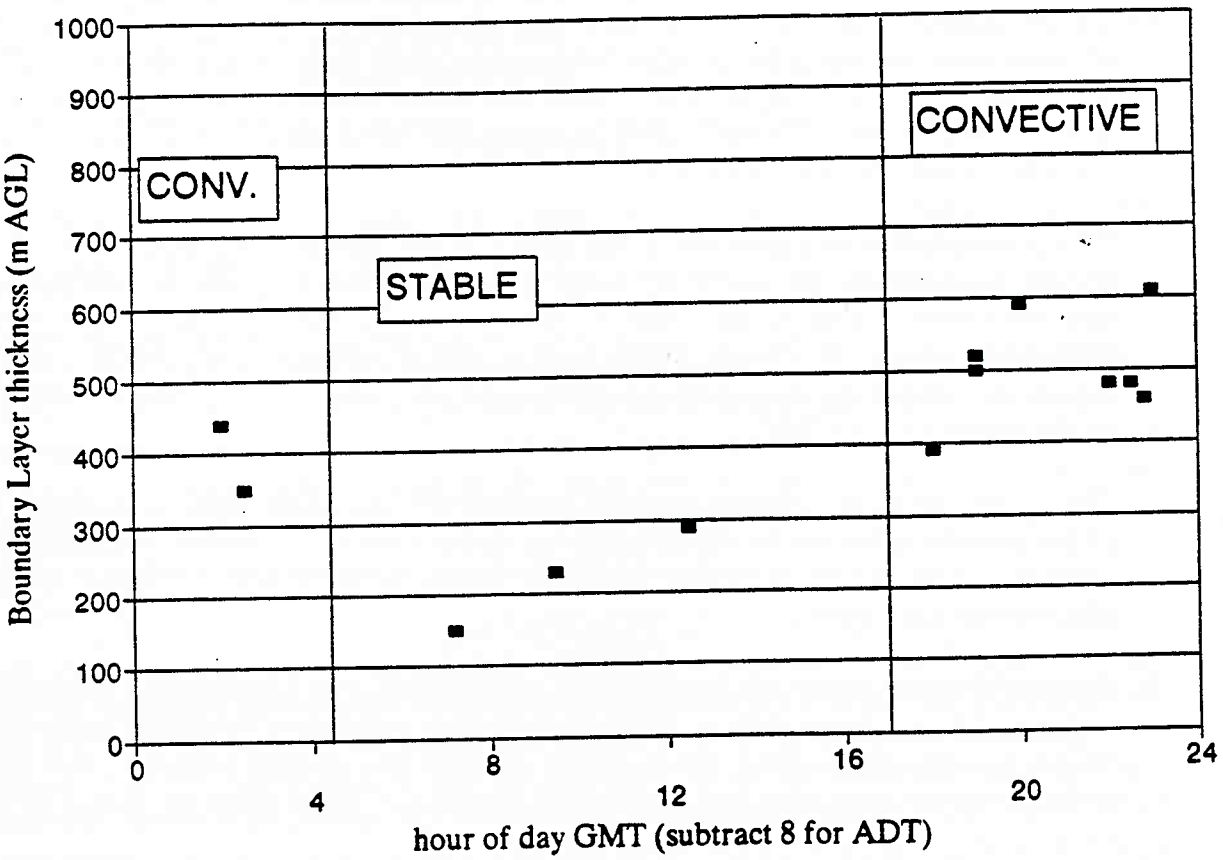

Figure 4. The measured boundary layer heights in meters (discrete points) during the ALFS study. The atmospheric boundary layer is divided into stable and convective periods. The transitions from convective to stable and stable to convective were assumed to occur at 1830 and 0900 Alaskan Daylight Time (ADT) respectively. The individual heights were determined by noting rapid changes in dew point and potential temperature with altitude and are only accurate to ± 50m.

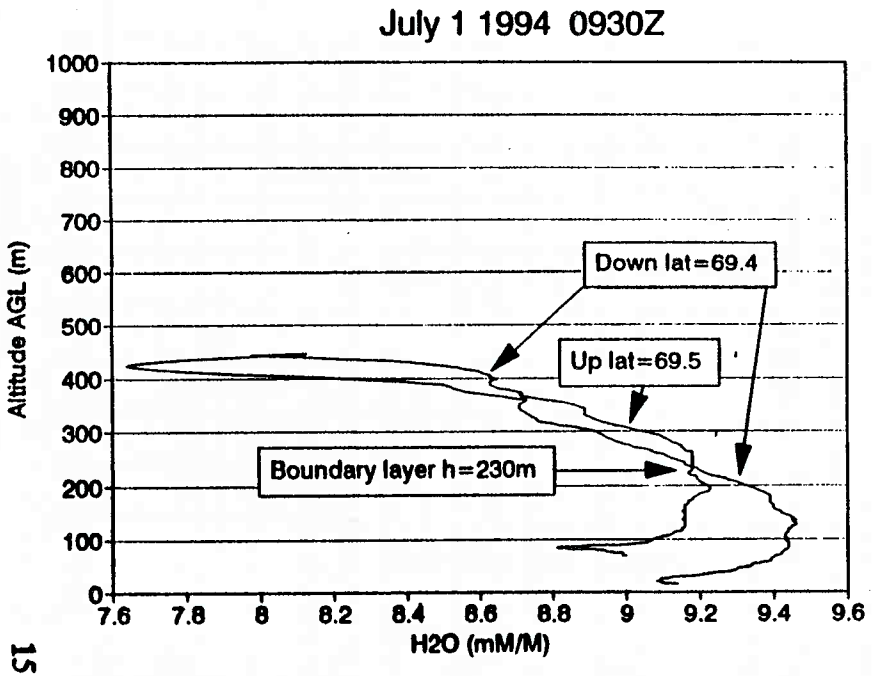

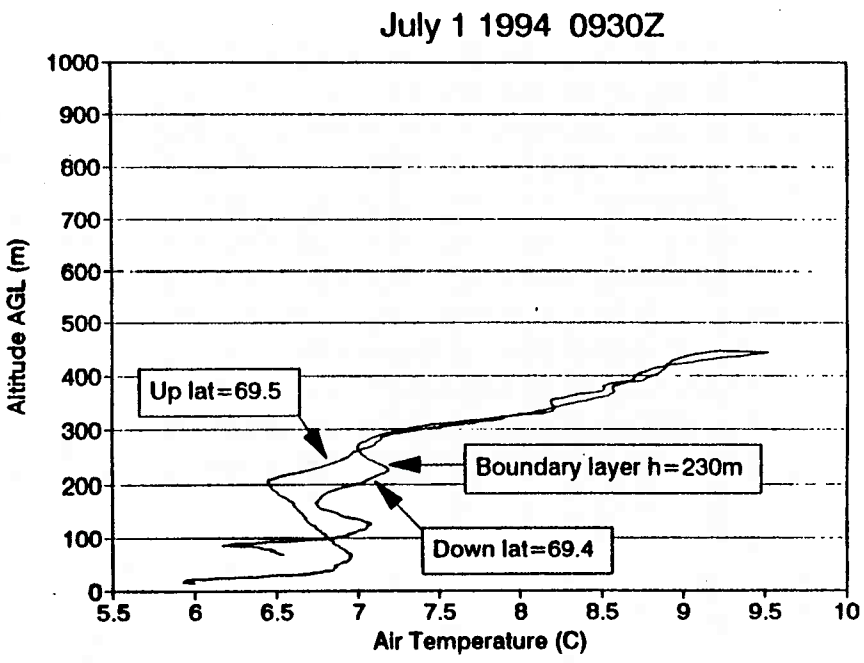

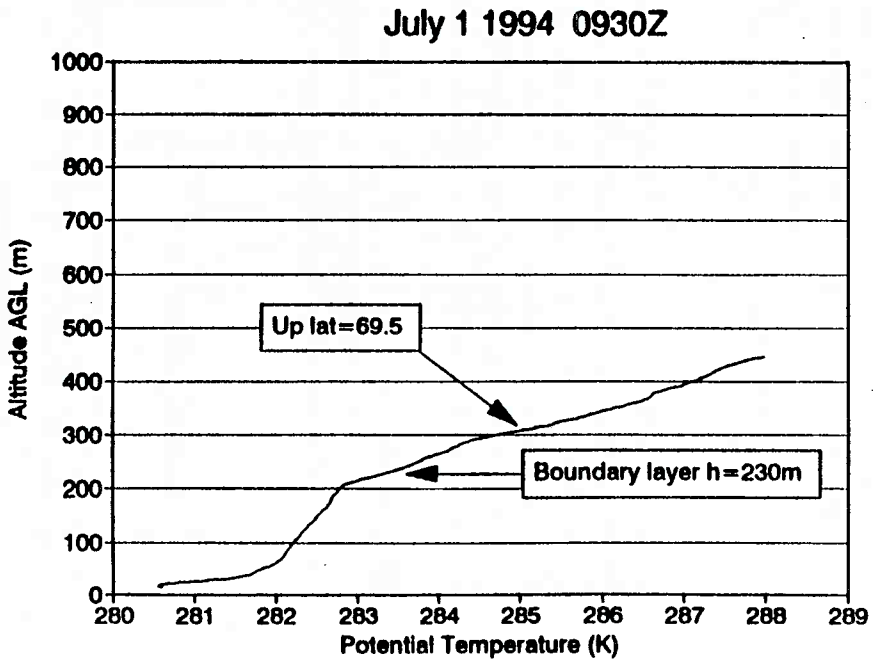

Figure 5a,b,c Profiles of water vapor, air temperature, and potential air temperature for a nighttime stable boundary layer. These measurements were made during an aircraft profile pattern, the approximate latitudes of the climbing and descending portions of the profiles are shown in the figures. These profiles were measured inland during clear weather and light winds from the north on July 1, 1994 at 0930 GMT (1:30 am Alaskan Daylight Time, ADT) along the North-South transect (Long. = 148°55').

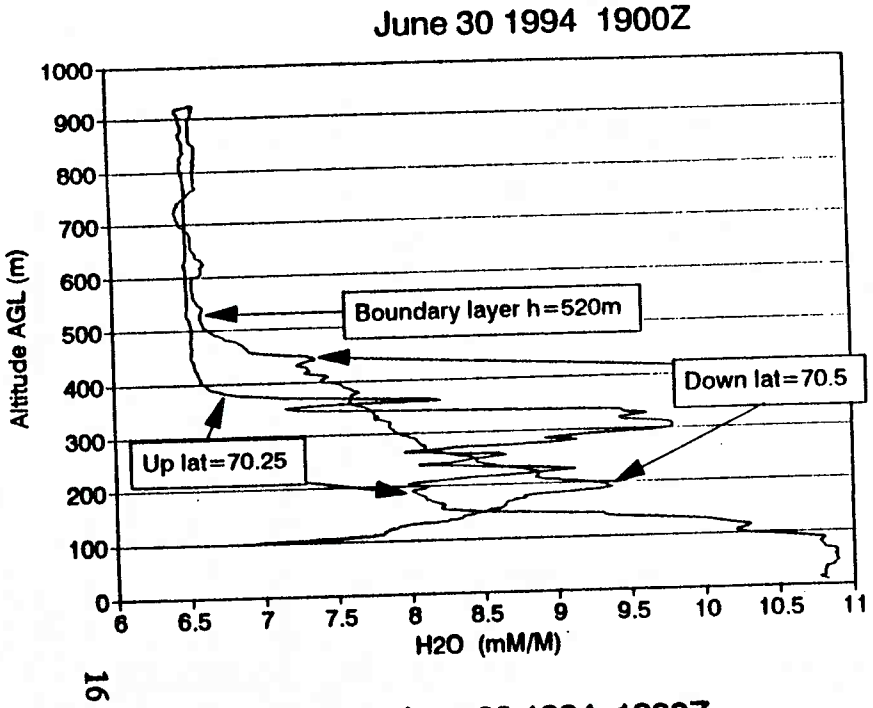

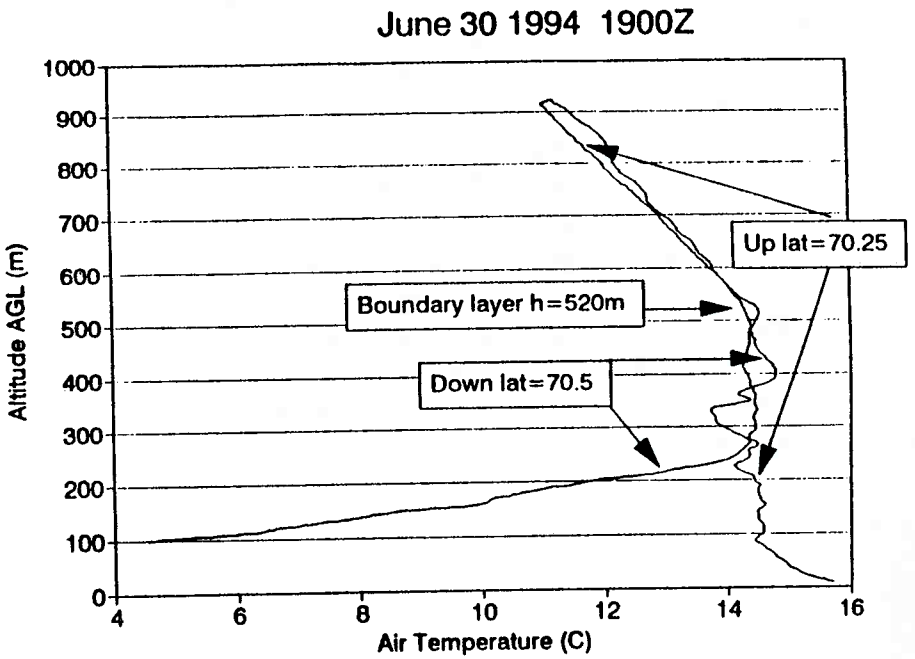

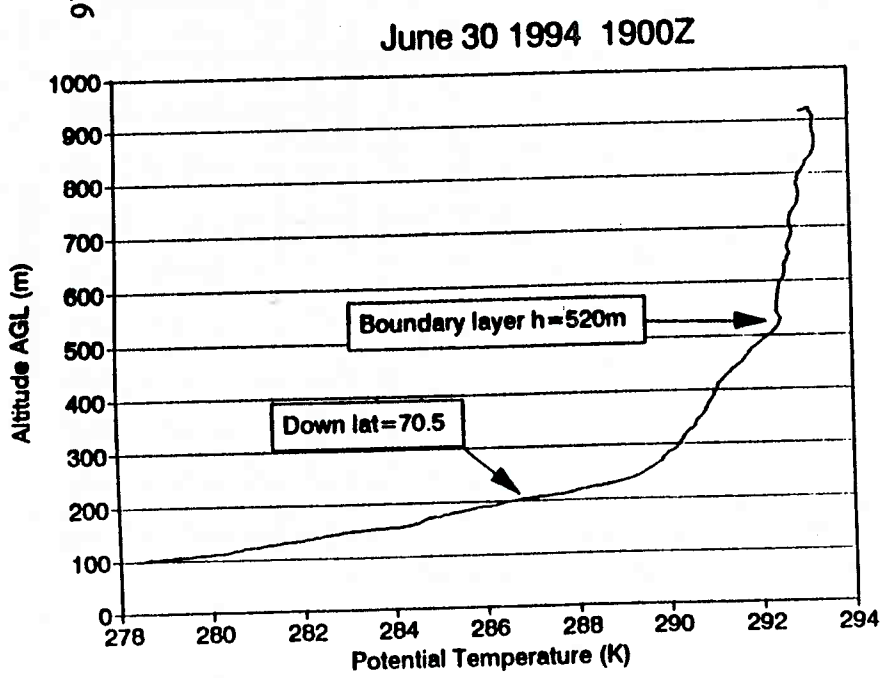

Figure 6a,b,c Profiles of water vapor, air temperature, and potential air temperature for a daytime convective boundary layer. These measurements were made during an aircraft profile pattern, the approximate latitudes of the climbing and descending portions of the profiles are shown in the figures. These profiles were measured during clear weather and light winds from the north on June 30, 1994 at 1900 GMT (11:00 am ADT) along the North-South transect (Long. = 148°55').

Figures 6a,b,c are boundary layer profiles measured during clear weather and light winds from the North on June 30, 1994 at 1900 GMT (11:00 am ADT). The ascending profile was initiated at a location (Lat. = 70.25°, Long. = 148.9°) ≈15 km inland from the Arctic Ocean. The descending profile ended at a location (Lat. = 70.5°, Long = 148.9°) ≈10 km offshore. The profiles show a boundary layer height of ≈520 m with water vapor, and temperature distributions constant above the boundary layer. The surface temperature differences between the Arctic Ocean (≈0° C) and the land (≈16° C) leads to rapidly changing distributions of temperature and water vapor within the boundary layer and large gradients as the aircraft transitions from the marine to the continental boundary layer.

These steep gradients require that the space trend be considered in the flux calculation, Eqn. 3. This was accomplished by the use of short time step running means in Eqn. 3. This effectively subtracts the mean without detrending the fluxes.

11. LONG TRANSECT AIRBORNE FLUX MEASUREMENTS

Just over 100 long-transect flux measurement flights were conducted during the summers of 1994 and 1995. Attempts were made to conduct flights at different times and weather conditions. However, the aircraft could not be operated safely in fog, moderate-heavy rain, or darkness as occurred during the early morning hours in mid-late August. Therefore, the aircraft data are biased towards what are commonly referred to as "sunny days". The aircraft data are also biased toward carbon dioxide sink activity as the summers of 1994 and 1995 were periods of above-average rainfall. This added water tends to inhibit the aerobic decomposition in the soils which is a carbon dioxide source to the atmosphere. Figure 7 shows histograms of north-south transect flight times for the three field studies. As shown in Fig. 7, the majority of the north-south transect flights occurred between 8am and 7pm (local Alaskan Daylight Time, ADT) and between 10pm and midnight (ADT). No north-south transects were flown from 11pm to 7am (ADT) during August due to periods of darkness in the early morning hours.

Figure 8 shows Normalized Difference Vegetation Indices (NDVIs) over the North-South transect for June 29 and August 17. NDVI is a common measure of vegetation activity and is computed from the red and Near InfraRed (NIR) spectral reflectances: (NIR-red)/(NIR+red). The red and NIR wavebands are used because strong red absorption by chlorophyll pigments and high NIR reflectance by multiple scattering within the intracellular air spaces surrounding the spongy mesophyll cells ensures a strong contrast in reflectance between these two wavebands (Jensen, 1983). High reflectance in NIR is indicative of vegetation amount (e.g., biomass or Leaf Area Index, LAI) and low red reflectance is indicative of high levels of intercepted Photosynthetically Active Radiation (PAR) which has been found to be correlated with plant production and CO_2 uptake.

(A) June 1994 Field Study

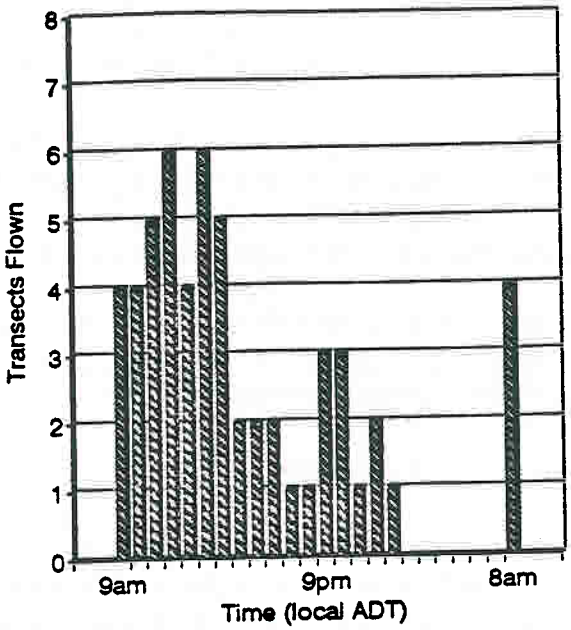

(B) June 1995 Field Study

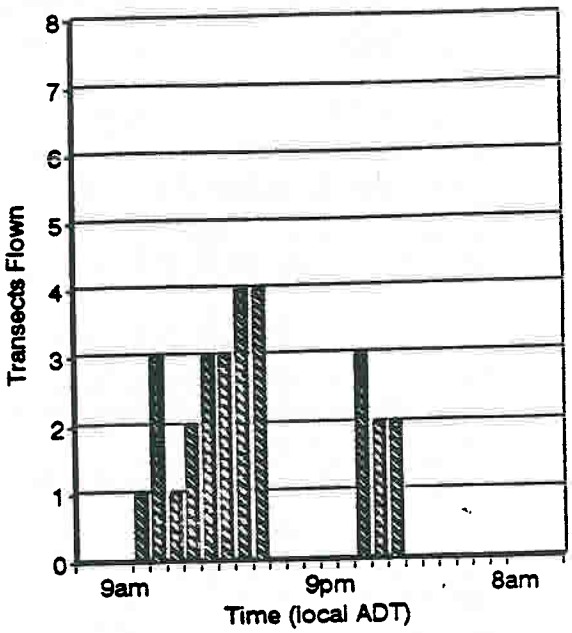

(C) August 1995 Field Study

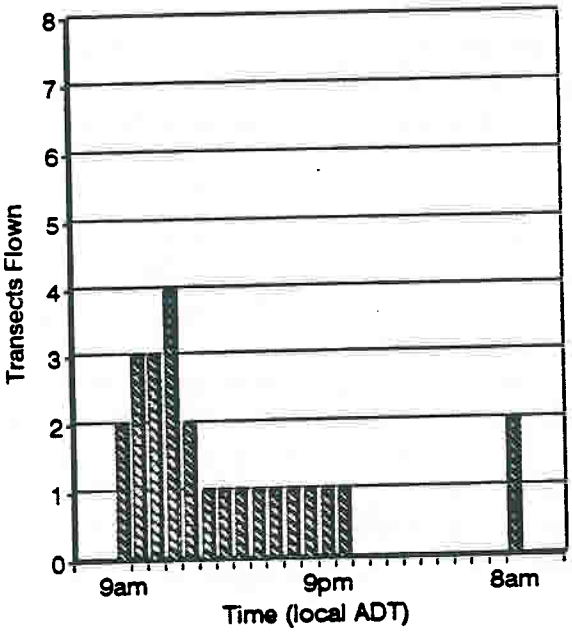

Figure 7a,b,c Histograms of north-south transect flight times for the three field studies. All times are local Alaskan Daylight Time (ADT).

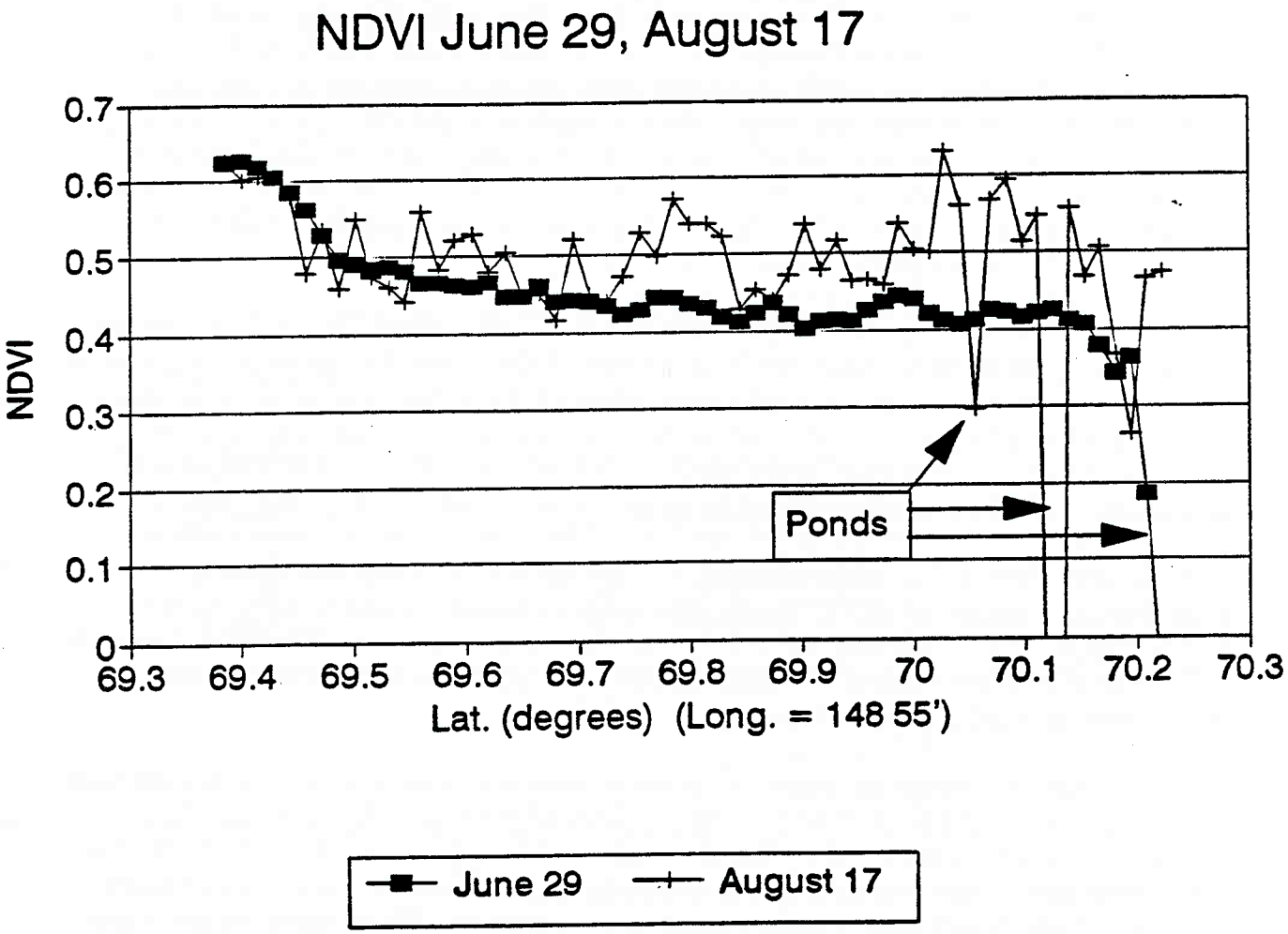

Figure 8. Normalized Difference Vegetation Indices (NDVIs) over the North-South transect for June 29 and August 17. NDVI is a common measure of vegetation activity and is computed from the red and Near InfraRed (NIR) spectral reflectances: (NIR-red)/(NIR+red). The north-south transect was flown at a constant Longitude of 148°55'. The location variable shown is North Latitude in decimal degrees.

NDVI was measured from an aircraft-mounted Exotech-100BX radiometer fitted with red and NIR filters corresponding to the spectral wavebands of the SPOT *(Système Probatoire d'Observation de la Terre)* satellite multispectral sensor. SPOT imagery has been acquired for future investigation into the relationship between NDVI at this scale to the scale of aircraft and hand-held radiometry. 15° Field of View (FOV) objectives were used so that at a flying height of 10m, Ground Resolution Elements (GREs) were nominally 2.6m in diameter. This GRE adequately included the inherent small-scale surface heterogeneity of tundra.

As shown in Fig. 8, in June the vegetation is flourishing in the warmer Brooks Range foothills (Lat. $\approx$ 69.4°) while the vegetation in the coastal plain (Lat. 69.6-70.2°) closer to the cooler Beaufort Sea is still recovering from winter and visually is a uniform brownish color. By August, the coastal plain vegetation is flourishing along with the foothills vegetation. The August NDVIs over the coastal plain show the heterogeneity of this coastal plain tundra landscape. The landscape is dominated by the topographical features of tundra polygons (3-50 m^2), frost boils (1-2 m^2) and ponds (5-100m^2) which causes the noise in the NDVI data.

Figure 9(a) shows average air temperatures for June and August. Overall summertime temperatures are warmer in the south and cooler in the north due to the cooling effects of the arctic ocean. The average difference between day (9am-9pm, local ADT) and night (9pm-9am) air temperatures was about 2°C. The summertime temperatures appear to be roughly constant in the southern foothills whereas the northern coastal plain (Lat. > 69.9°) is clearly warmer in August than in June. Figure 9(b) shows average ground surface temperatures for June. The average daytime June surface temperatures were 1-2°C colder than the average air temperatures and show a clear drop from an average of 12.1°C at the southernmost transect point to 5.2°C at the northernmost point. Whereas the average daytime August surface temperatures were 0-7°C warmer than the average air temperatures. No nighttime surface temperature measurements were made in August.

The difference in surface temperatures between June and August is due to the increase in thawed layer depth from June to August. Coastal plain thaw layer depth measurements were conducted by San Diego State University researchers in 1994. On the coastal plain, thaw layer depths were repeatedly measured in a low center tundra polygon, a high center tundra polygon, and two ice wedges. These three surface types are conspicuous features of the average North Slope coastal plain topography (Walker and Acevedo, 1987). The measured thawed layer depths are shown in Fig. 10.

In late June (Julian days 170-180), the thawed layer deepened at an average rate of 0.54 cm/day whereas in mid-August (Julian days 225-235) the average deepening rate was 0.15 cm/day. The difference in thawing rates and therefore the soil heat flux is due to the greater thawed layer depth in August effectively insulating the top surface of the

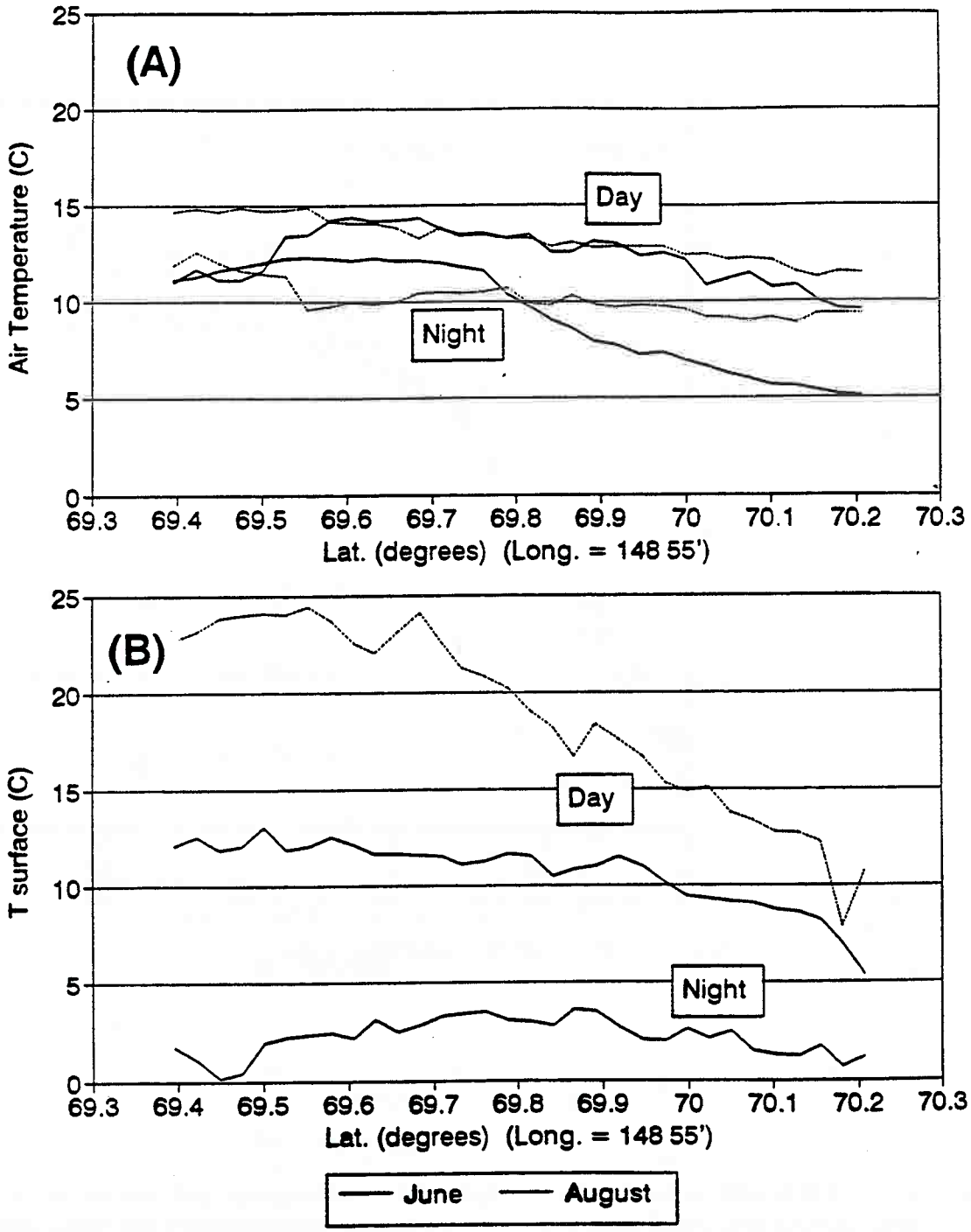

Figure 9a,b Average air temperature (°C) at 10m AGL (A), from the north-south transect, June and August 1995. Daytime data represent all flights occurring between 9am and 9pm Alaskan Daylight Time (ADT). Nighttime data represent those flights between 9pm and 9am ADT. Average surface temperature (°C) (B) from the north-south transect, June and August 1995. Surface temperatures for the mid-August nighttime were not measured due to instrument problems.

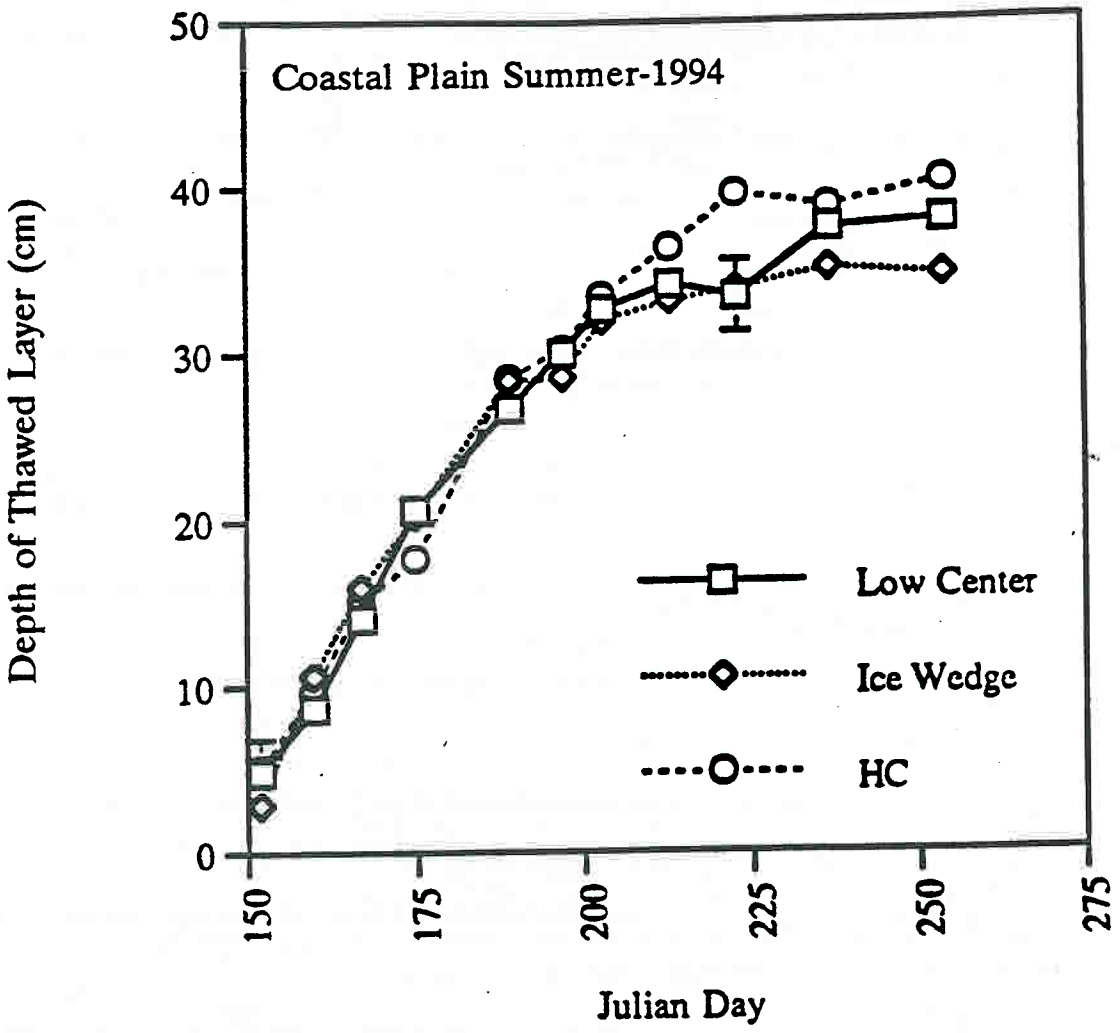

Figure 10. Measurements of thawed layer depths made by San Diego State University during the 1994 summer. The three curves represent the thaw depths of a Low Center polygon, an Ice Wedge, and a High Center (HC) Polygon. The aircraft operation periods were in late June (Julian days 170-180), when the average permafrost melting rate was 0.54 cm/day, and mid-August (Julian days 225-235) when the average melting rate was 0.15 cm/day.

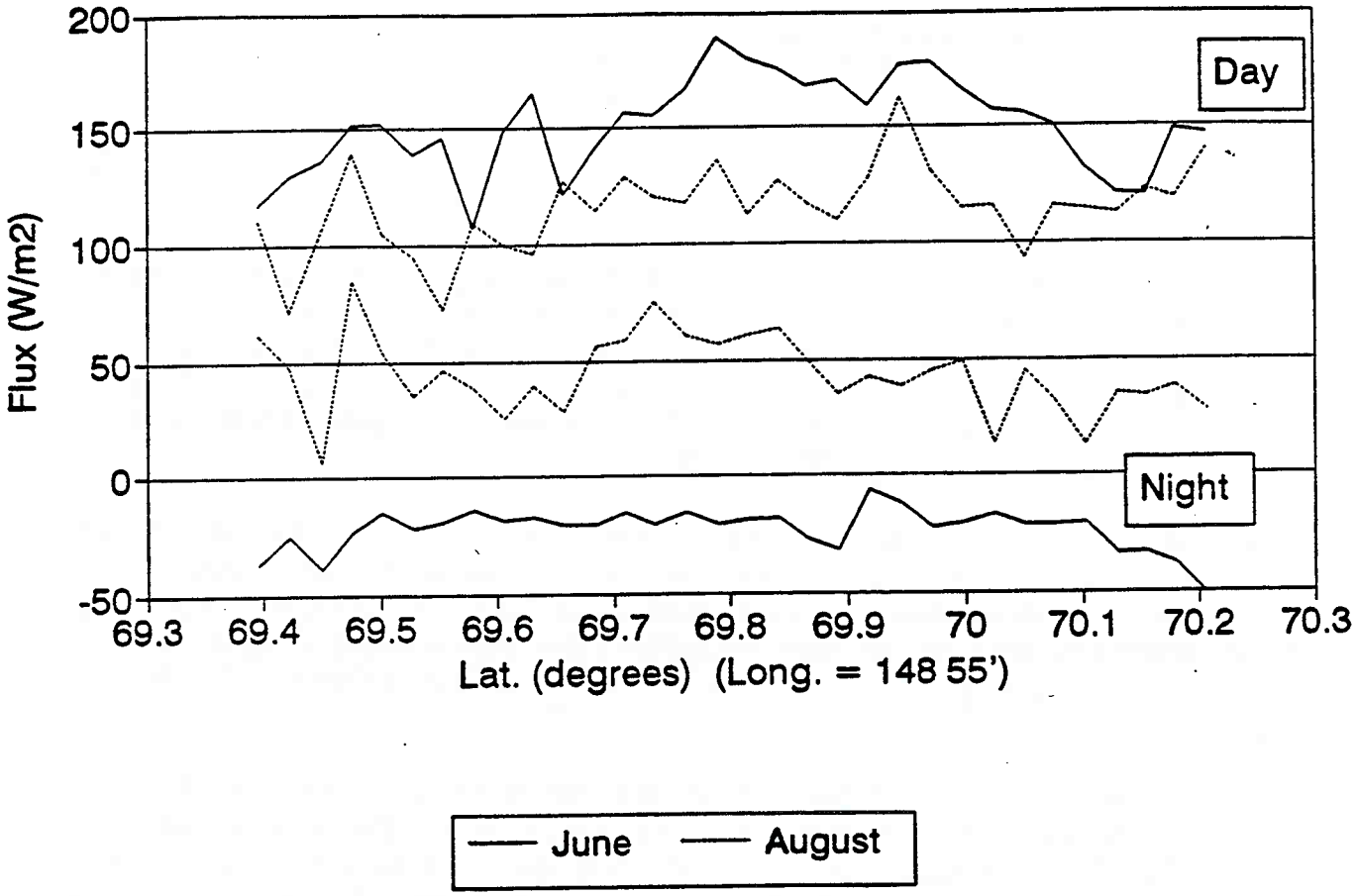

Figure 11. Average soil heat flux, G_t (W/m^2), from the north-south transect, June and August 1995. G_t was not directly measured but was calculated by the summation of the net radiation flux, R_t, the sensible heat flux, H_t, and the latent heat flux (water vapor flux), LH_t, ($R_t+H_t+LH_t$). A positive flux indicates heat flux into the soil.

permafrost. This organic-rich soil insulation also induces the higher surface temperatures in August. As was shown in Figs. 8 and 9, the average daytime surface temperatures in August were 1-7°C higher than the air temperatures, whereas the June surface temperatures were 1-2°C cooler than the air temperatures.

The soil heat flux (Fig. 11), G_f, was taken as the sum of the net radiation flux (R_f), the sensible heat flux (H_f), and the latent heat flux (water vapor flux) (LH_f). Aircraft measurements of NDVI and soil heat flux ($R_f+H_f+LH_f$) along the transect show that this soil heat flux is a strongly correlated to vegetation and terrain features (such as thermokarst lakes). The comparison between NDVI and G_f measurements will not be exact because of differences in footprint sizes and locations. The footprints for H_f and LE_f, used to calculate G_f, are on the order of 1 km^2 and are located upwind of the aircraft location. In contrast, NDVI Ground Resolution Elements are about 2.6 m in diameter and are located directly beneath the aircraft.

Latent heat flux or water vapor flux, LH_f, is shown for the north-south transect in Fig. 12 for daytime and nighttime periods. As expected the fluxes are higher during the daytime hours. In June during the nighttime LH_f is very low due to a cold surface caused by the thin thawed layer ($\approx$20 cm) over frozen soil. In nighttime August, the thawed layer is much thicker ($\approx$50 cm) and the surface retains enough heat for significant evapotranspiration. Daytime latent heat flux is slightly higher in the south than in the north. This is thought to be due to higher concentrations of shrubs and the resulting increase in Leaf Area Index (LAI) in the south. A similar north-south trend has been observed by Eugster (et al., 1996).

Sensible heat flux, H_f, is shown for the north-south transect in Fig. 13 for daytime and nighttime periods. Again, as with latent heat flux, the fluxes are higher during the daytime hours. In nighttime June the sensible heat fluxes are nearly zero, again due to the thin thawed layer and the very cold surface. Sensible heat flux is roughly the same magnitude as the latent heat flux, but unlike the latent heat flux no north-south trend is discernable.

Photosynthetically Active Radiation ,PAR, is shown in Fig. 14. Average PAR during the daytime (9am-9pm) was roughly constant at $\approx$800 W/m^2. The average nighttime (9pm-9am) PAR for August was greater than that measured for June. This sample bias is due to the short period (3-4 hours) of darkness during the mid-August nights when the aircraft could not be operated because of safety concerns. In June, sunlight is twenty four hours a day.

Carbon dioxide fluxes are shown in Figs. 15, 16, and 17 for the daytime north-south transect, the nighttime north-south transect and the daytime east-west transect, respectively. A negative value indicates that the surface is a sink for atmospheric carbon dioxide. The daytime June fluxes show almost no difference from 1994 to 1995 and are reasonably uniform throughout the north-south transect. The daytime August

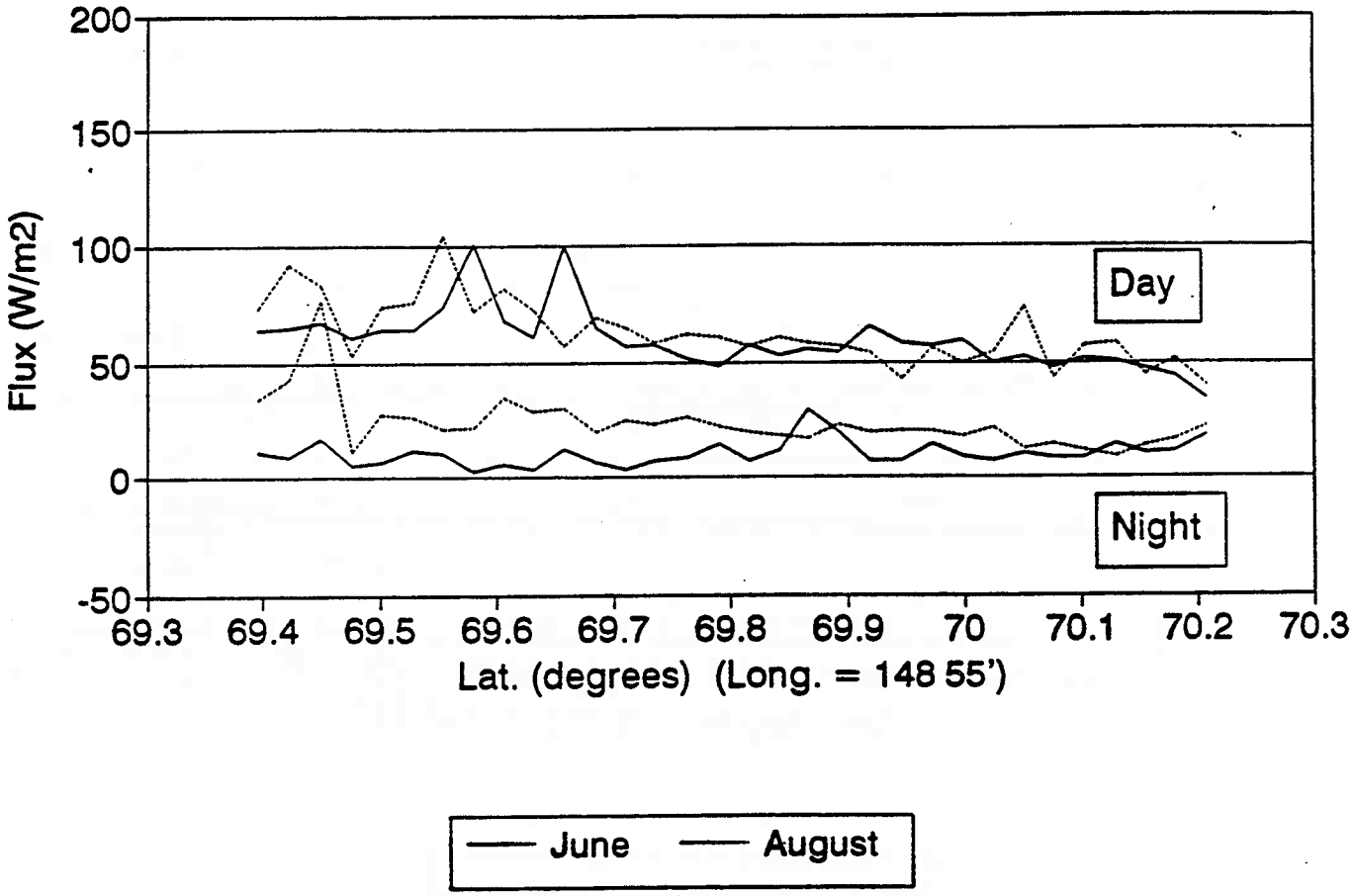

Figure 12. Average latent heat flux, LE_f (W/m^2) from the north-south transect, June and August 1995. Daytime fluxes show an increasing trend southward. This trend was also observed independently by Eugster *et al.* (1996).

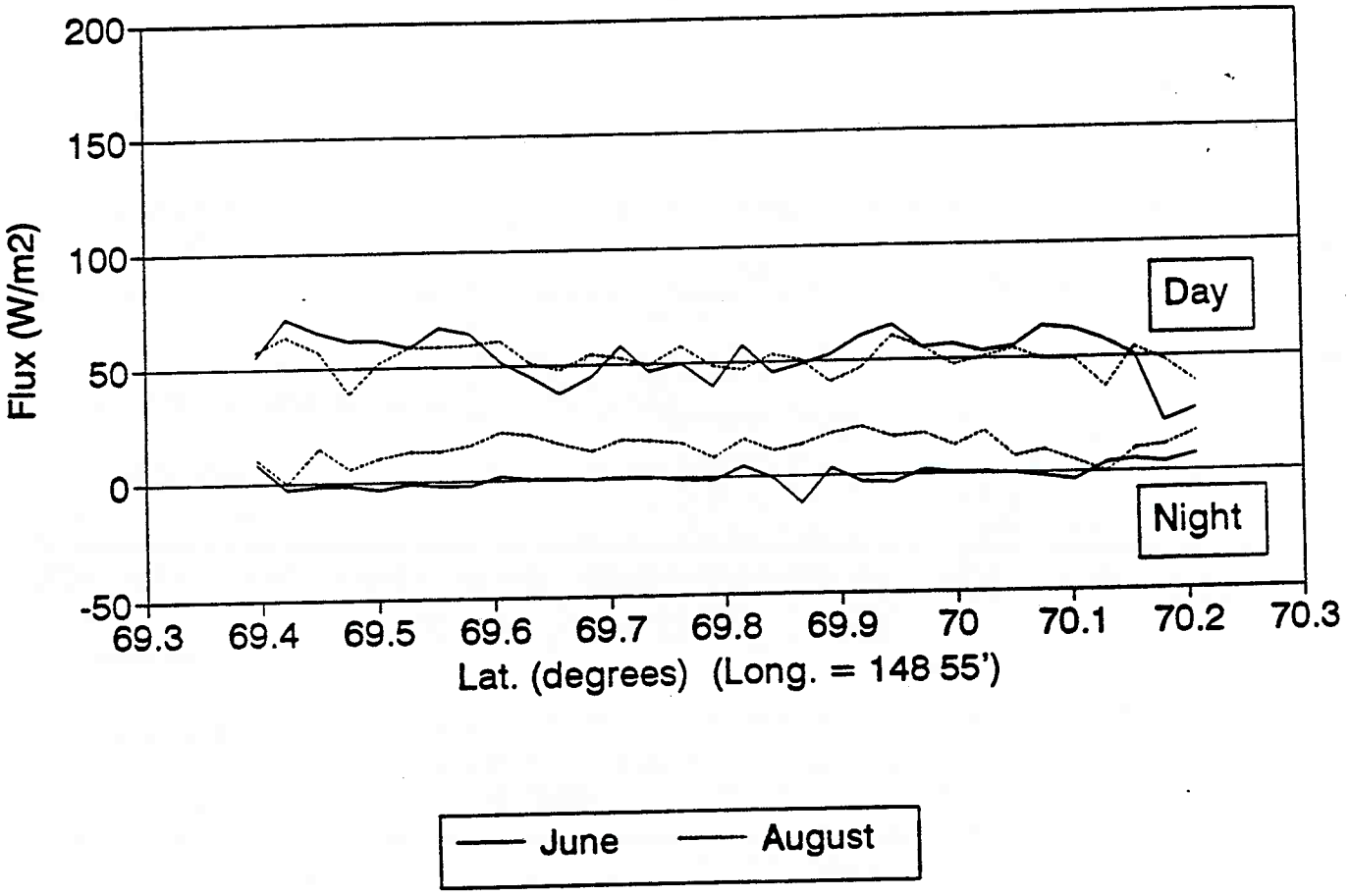

Figure 13. Average sensible heat flux, H_t (W/m^2) from the north-south transect, June and August 1995. A positive flux indicates heat transfer from the surface to the atmosphere.

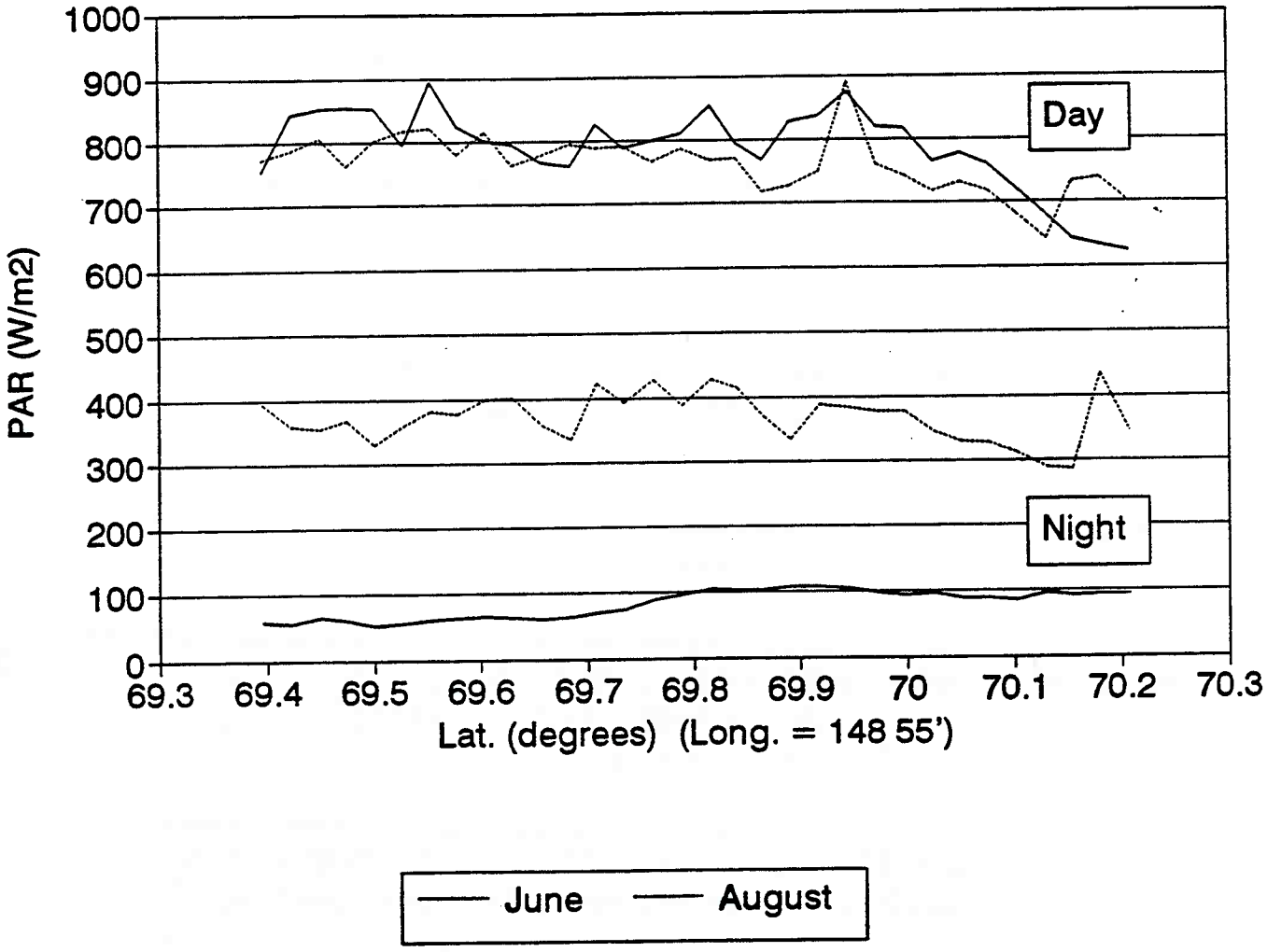

Figure 14. Average incoming Photosynthetically Active Radiation, PAR (W/m^2), from the north-south transect, June and August 1995. The average nighttime PAR for August was greater than that measured for June. This was due to the short period (3-4 hours) of darkness during the mid-August nights when the aircraft could not be operated because of safety concerns.

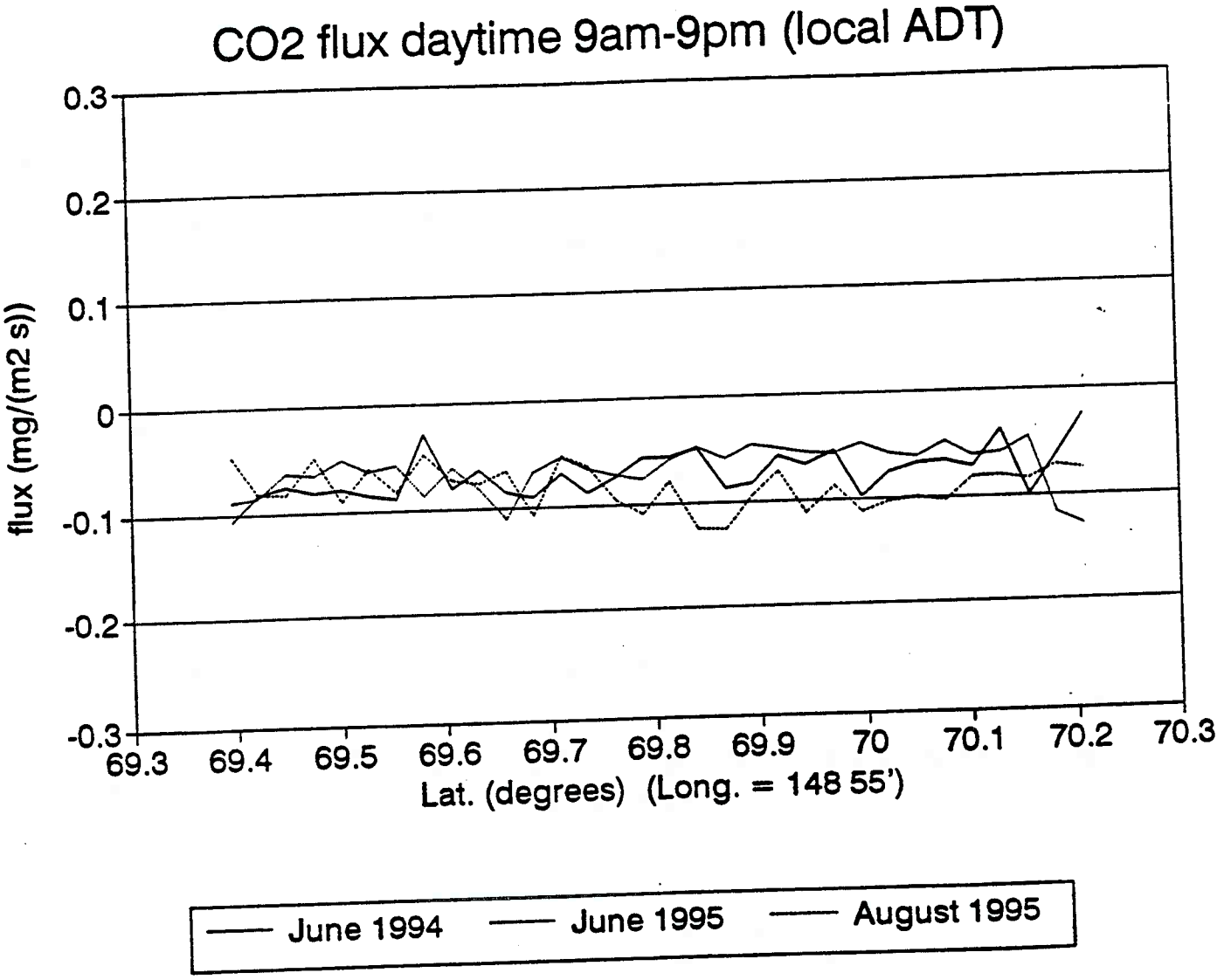

Figure 15. Average carbon dioxide flux ($mg(CO_2)\ m^{-2}\ s^{-1}$) from the coastal plain. Data are from the north-south transect during the daytime (9am-9pm, local ADT). Data from June 1994, June 1995, and August 1995 are shown. A negative value indicates that the surface is a sink for atmospheric carbon dioxide

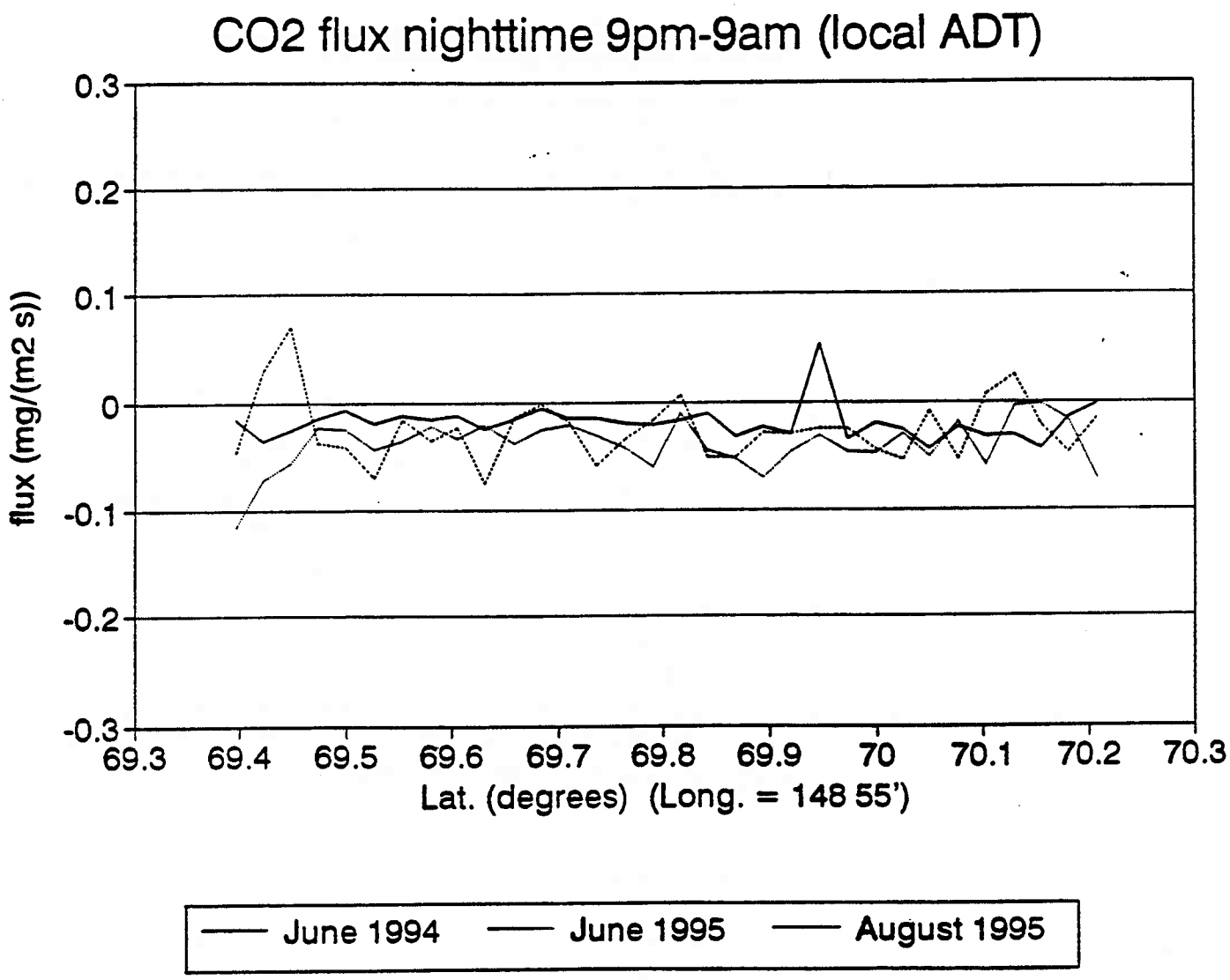

Figure 16. Average carbon dioxide flux ((mg(CO_2) m^{-2} s^{-1}) from the coastal plain. Data are from the north-south transect at night (9pm-9am, local ADT).

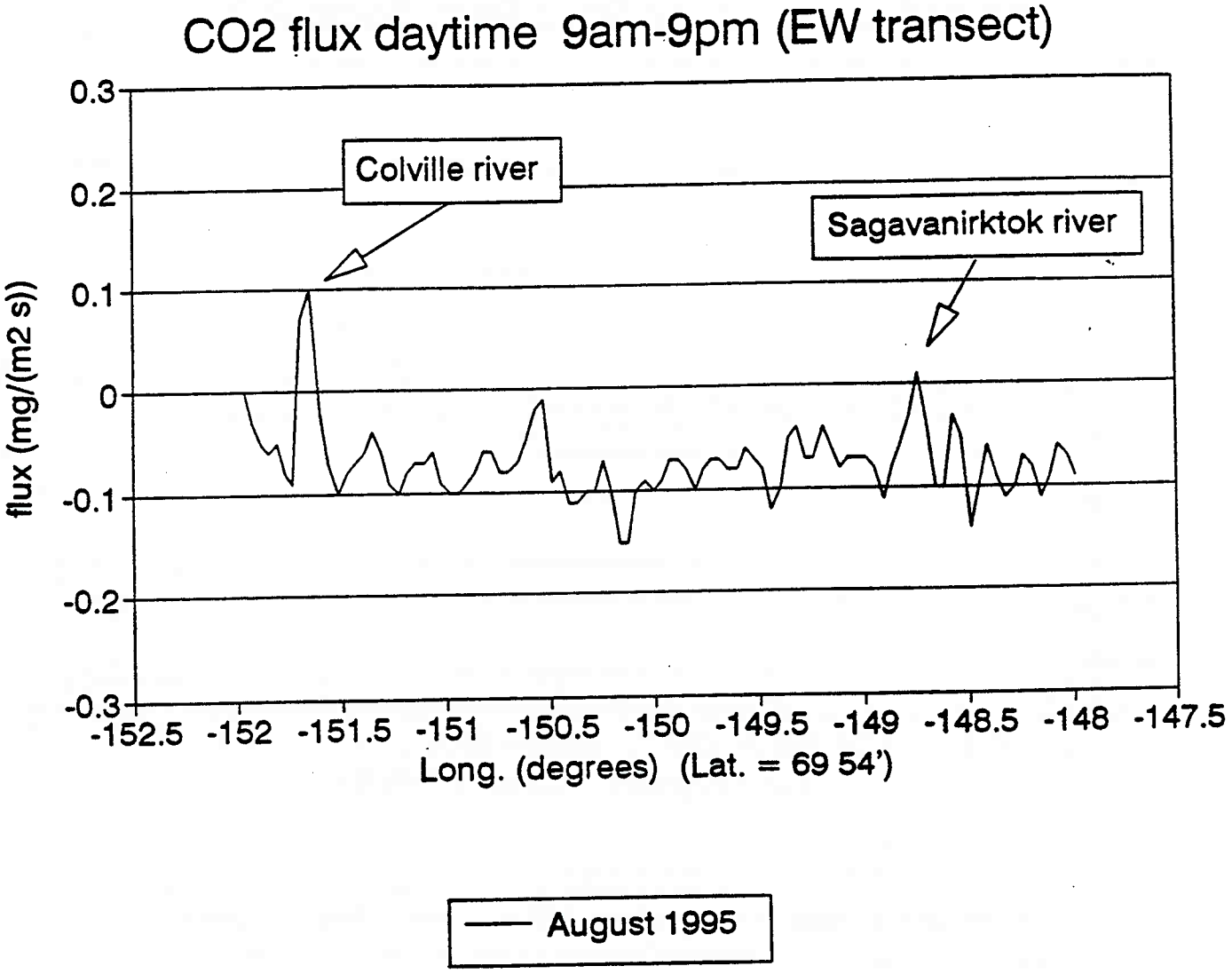

Figure 17. Average carbon dioxide flux ($mg(CO_2)\ m^{-2}\ s^{-1}$) from the coastal plain. Data are from the east-west transect. The east-west transect was sampled only during the August 1995 daytime hours.

flux shows a slightly greater sink in the north when compared to the June fluxes. This is to be expected as by August the vegetation growth in the northern study area has caught-up with the vegetation in the southern portion (See NDVI in Fig. 7).

Nighttime fluxes (Fig. 16) are lower in magnitude than the daytime fluxes mainly due to less photosynthetic activity. Small source areas are scattered throughout the transect. These source areas are thought to be medium size lakes which vary from year to year in size and shape. Wind speed and direction also affects the size and location of the flux footprints; including and excluding small and medium size lakes in the flux results.

Carbon dioxide flux for the daytime east-west transect (Fig. 17) shows more heterogeneity than the daytime flux for the north-south transect. This is due to the distribution of rivers and streams which flow predominately from south to north. The two major rivers crossed by the east-west transect show up as the only source locations. This is a clear example where the aircraft measurements have been particularly successful in resolving landscape-level patterns of flux as tundra waters are constant sources of CO_2 to the atmosphere (Hobbie, 1996).

Overall, the east-west and north-south transect CO_2 fluxes show uniformity throughout the coastal plain despite north-south gradients in temperatures and vegetation NDVI. In addition, the east-west transect results are similar to the north-south transect results at the crossing latitude (69°54'). This uniformity and the similarity between 1994 to 1995 flux measurements makes extrapolation to the circumpolar arctic a possibility.

12. TOWER RESULTS

Tower eddy correlation measurements allow a continuous measurement of integrated flux over a local area. These local areas are sufficiently large to integrate the different fluxes due to local vegetation and microtopographic gradients (e.g. tundra polygons, small ponds, etc.). Aircraft eddy correlation measurements allow determination of CO_2 flux over transects covering extensive areas. Currently aircraft appear to be the best direct approach to assess the actual flux over large landscape units. The combination of eddy correlation towers to give continuous records in time and eddy correlation aircraft to give large scale continuous records in space has been extensively utilized in this study.

The "24 mile" tower site (See Fig. 3) was operated by NOAA ATDD from June 24 to July 4, 1994. San Diego State University subsequently took-over the "24 mile" site and constructed their tower approximately 100m from the NOAA ATDD site. Results from June 24 to July 4 are shown in Fig. 18. The average measured CO_2 flux was +0.029 $mg(CO_2)\ m^{-2}\ s^{-1}$, indicating that for this location and time period the tundra surface was a mild source for atmospheric CO_2. While the average flux was positive, the tower measurements fluctuated between positive (source) and negative (sink) during every 24 hour period. This a further indication of the sensitive carbon balance of the arctic tundra.

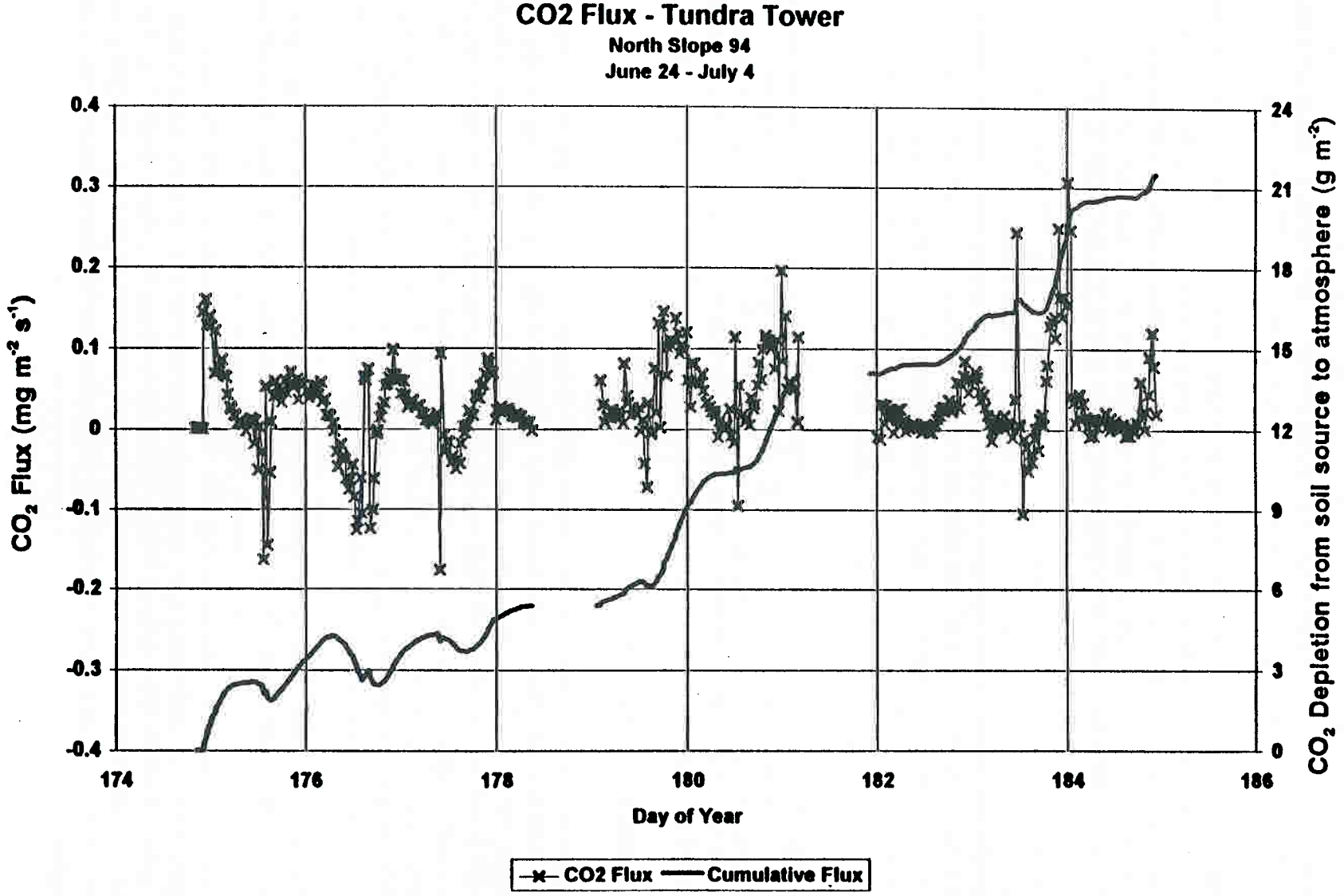

Figure 18. Results from the NOAA ATDD operated "24 mile" tower from June 24 to July 4. Shown are 30 minute average fluxes (+ source, - sink) and the cumulative carbon dioxide depletion from the surface. The average CO_2 flux shown is 0.029 mg(CO_2) m^{-2} s^{-1}. Gaps in the data are periods when the tower was not in operation.

Figure 19 shows a comparison between tower and aircraft net CO_2 flux estimates made between June 20 and 25, 1995. Aircraft estimates are from individual transect flux averages within $\pm$ 10 latitudinal minutes of the San Diego State University "Happy Valley" tower site (See Fig. 3).

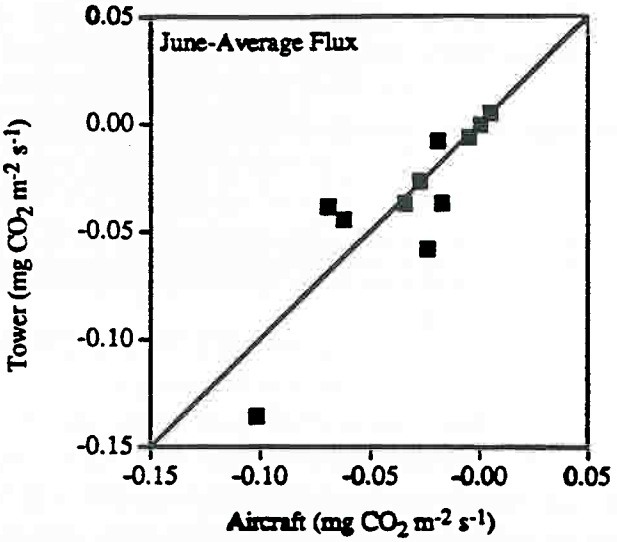

Figure 19. Comparison between tower and aircraft net CO_2 flux estimates made between June 20 and 25, 1995. Aircraft estimates are within $\pm$ 10 latitudinal minutes of the "Happy Valley" tower site.

13. REPRESENTATIVENESS OF MEASUREMENTS

The value of the ALFS study lies in the ability to extrapolate the results of other arctic tundra regions. Methods for extrapolation include a statistical analysis of the contributing elements to measured fluxes, remote sensing to identify landscape variables that can be used to estimate state of activity, and modeling of ecosystem processes which affect the trace gas fluxes. The validity of the extrapolation of the observed fluxes increases as similarities of ecology and environment are identified and decreases as differences are identified. Similarities of the study area to the remainder of the circumpolar tundra are:

1. Wet/moist non-acidic tundra type is a predominate circum-polar tundra type (Walker, 1996).

2. The latitude of the coastal plain is a rough median for wet/moist non-acidic tundra.

3. Mid-summer precipitation and temperatures are characteristic for circumpolar wet/moist nonacidic tundra (Kane et al., 1996).

4. Vegetation species are also characteristic (Walker, 1996).

Differences between the study area and the remainder of the circum-polar tundra are:

1. Arctic rivers elsewhere develop large springtime ice dams which effect soil composition by flooding and erosion. An example of this erosion comes from carbon dating of the top 1m of soil. On the Yukon river delta the median soil age is 1200 years (Sedinger and Ruess, 1996) whereas on the Sagavanirktok river delta (in the study area) the median age is 4000 years (Ping, 1996).

2. Other coastal tundra regions do not have East-West running mountain ranges, such as the Brooks Range.

3. Most of the remaining circum-polar tundra receives more wintertime snow fall. Increased snow depth minimizes wintertime plant desiccation but causes longer melting periods and shorter growing seasons.

14. DISCUSSION

The average aircraft CO_2 flux measurements show that tundra was an overall sink for atmospheric CO_2 at an average daily rate of -0.043 mg(CO_2) $m^{-2} s^{-1}$. The tundra was shown to be a uniform sink during the daytime (9am-9pm ADT) and a mixture of source and sink areas during the night (9pm-9am). The NOAA ATDD continuous "24 mile" tower measurements from June 24 to July 4, 1994 show that the tundra was a mild source of CO_2 to the atmosphere at a rate of +0.029 mg(CO_2) $m^{-2} s^{-1}$. The polarity of these results demonstrates the capricious nature of the tundra CO_2 balance. In comparison, recent measurement of CO_2 fluxes from temperate broad leaf and boreal forest environments showed mean surface/atmosphere fluxes of -1.52 and -0.49 mg(CO_2) $m^{-2} s^{-1}$ respectively (Baldocchi and Vogel, 1996).

From the comparison of these orders of magnitude between forest and tundra fluxes, it could be assumed that the tundra CO_2 flux is equal to zero. This possible result alone may be significant as historically the tundra has been a sink for atmospheric CO_2 as evident from the immense carbon stocks within tundra soils. The possible change from this historical sink activity may be difficult to detect but is still significant in the long term.

Presently, global change in the form of rising temperatures and increased precipitation may be affecting the carbon balance of the arctic tundra. The definitive detection of tundra change from an historical sink to a current source has not been made in this NOAA ATDD two-year study period. There are many reasons for this:

1. The aircraft is limited in time of use due to weather and darkness.
2. The towers are limited in footprint area.
3. 1994 and 1995 were heavy-precipitation years.

4. The tundra CO_2 flux rates (positive or negative) are very small compared to those of other ecosystems.

The work of San Diego State University researchers from 1983 to the present indicates that the tundra in the last 13 years has been an overall source of atmospheric carbon dioxide; that this change coincides with recent climatic variations in the arctic, and suggests a positive feedback of arctic ecosystems on atmospheric CO_2 and global change. Their Alaskan north slope study results from 1983 to 1992 indicate a loss of carbon from tussock tundra of 156 g m^{-2} y^{-1}, and from the wet tundra of 34 g m^{-2} y^{-1} (Oechel *et al.*, 1993). If these rates are representative of the circumpolar tundra, then they equate to a net annual global loss of carbon as CO_2 to the atmosphere, and when combined with measured winter fluxes (Oechel *et al.*, in press), overall losses of CO_2 from tundra to the atmosphere may be 0.7 GtC year (Oechel *et al.*, *in press*).

From these two-year NOAA ATDD findings it is impossible to confirm or deny these longer term findings. Depending on the nature, rate, and magnitude of global environmental change, the arctic may have a continued positive or a negative feedback on global change. From the longer terms results of the San Diego State University research and others, it is likely that northern ecosystems will be an increasing source of CO_2 and will have a positive feedback on the global climate (Billings, *et al.*, 1982; Post, 1990; Oechel and Billings, 1992).

15. PROBLEMS ENCOUNTERED

The major problems encountered in the determination of the tundra fluxes were the Prudhoe Bay oil facility CO_2 emission plumes and the non-horizontal advection winds in the Brooks Range foothills. The main north-south transect ran from 69.0° to 70.5° N Lat. Due to these flux measurement problems, the data presented in the previous sections were from 69.4° to 70.2° N Lat., roughly the area of the gently sloping coastal plain. Omitted were the areas around the oil production facilities (north of 70.2° Lat.) and the Brooks Range foothills (south of 69.4° Lat.). The average fluxes over the entire north-south transect are shown in Fig. 20.

The Prudhoe bay oil fields emit large quantities of carbon dioxide from the combustion of natural gas in power generation and excess gas flaring. A single measurement of the emissions plumes gave an emissions rate of $1.3X10^3$ metric tons (C) $hour^{-1}$ (Brooks et al., 1996). In the northern section of the main transect, the aircraft flew in and out of the large emissions plumes of the oil production facilities. Changes in wind direction did not relieve this problem, as oil facilities existed on both sides of the main north-south transect. The passage of the aircraft through the plumes overwhelmed the changes in CO_2 concentration due to turbulent eddy motion. These plumes adversely affected the tundra flux measurements north of 70.2° N Latitude as shown in Fig. 20.

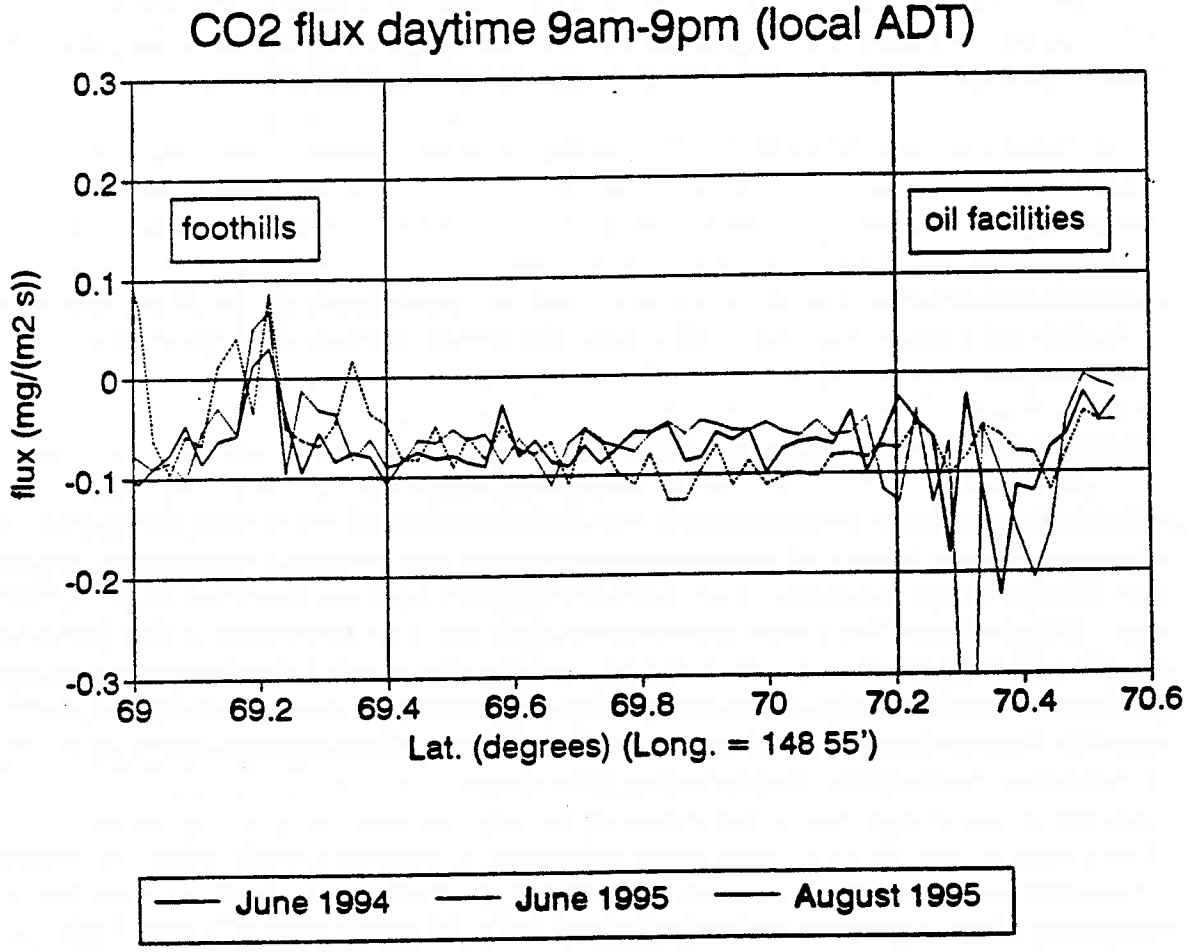

Figure 20. Expanded average carbon dioxide flux ($mg(CO_2)\ m^{-2}\ s^{-1}$) from the coastal plain. Data are from the north-south transect during the daytime (9am-9pm, local ADT). Data from June 1994, June 1995, and August 1995 are shown. A negative value indicates that the surface is a sink for atmospheric carbon dioxide

The second major problem encountered was the rolling foothills of the Brooks Range. The total vertical flux of any stable species is the sum of the advection (the product of the average vertical wind and the species concentration) and the eddy flux. In standard eddy correlation methods, the advection term is often assumed negligible, with the assumption that the average vertical velocity close to the surface is zero. Over rolling foothills the vertical velocities near the ground are non-zero, and, in this case, overwhelm the eddy vertical velocities. The effects of the foothills are also evident in the CO_2 flux results shown in Fig. 20.

16. SUMMARY AND RECOMMENDATIONS

Repeated aircraft measurements along a fixed transect are a good means of obtaining long-term (3-4 weeks) spatial averages of vegetation indices and mass (CO_2 and H_2O) and energy fluxes. Superposition of multiple passes, each short enough to resolve surface features of interest, appears to be the most suitable method for sampling by airplane. Accurate positioning using the Global Positioning System insures confidence in the superpositions. The aircraft measurements allow model extrapolation based on vegetation indices and energy fluxes of limited land based point measurements of tundra topography, especially in remote or otherwise inaccessible areas.

Overall, the east-west and north-south transect CO_2 fluxes show uniformity throughout the gently sloping coastal plain despite north-south gradients in temperatures and vegetation NDVI. This uniformity and the similarities between 1994 to 1995 flux measurements makes extrapolation to the circumpolar arctic a possibility.

The results show that the summertime tundra can be both a sink and a source for atmospheric carbon dioxide depending on location and time of day. While the tundra historically is a sink for CO_2, recent climatic trends make have changed the tundra into an overall source of CO_2. This two-year study can only conclude that the tundra carbon flux is very close to zero, and that there exists a significant possibility that the tundra may now be an overall source of CO_2 to the atmosphere.

Future measurements of carbon dioxide flux should be conducted farther from large sources of anthropogenic CO_2 emissions. In this study the emissions plumes from the Prudhoe Bay oil production facilities overwhelmed the tundra fluxes in the oil field areas. Transect flights over rolling foothills should also be avoided, as eddy correlation methods require that the average vertical velocity close to the surface is zero. Over rolling foothills the vertical velocities near the ground are non-zero which precludes an accurate determination of the flux.

17. ACKNOWLEDGMENTS

We would like to acknowledge the San Diego State University researchers who brought this program together; Walt Oechel, Doug Stow, Allen Hope and George Vourlitis. We would also like thank Roger Dahlman of the Department of Energy for his continued support of our research efforts.

This research was performed as part of the National Science Foundation Land-Atmosphere-Ice Interaction (LAII) study. Additional funding and logistical support was provided by the U.S. Department of Energy, Environmental Sciences Division, Office of Health and Environmental Research and BP Exploration (Alaska) Inc. This work was performed while the primary author held a National Research Council-NOAA Research Associateship.

REFERENCES

Baldocchi, D.D., B.B. Hicks, and T.P. Meyers, 1988. Measuring biosphere-atmosphere exchanges of biologically related gases with micrometeorological methods. Ecology. 69: 1331-1340.

Baldocchi, D.D. and C.A. Vogel, 1996. Energy and CO_2 flux densities above and below a temperate broad-leaved forest and a boreal pine forest. Tree Physiology. 16: 5-16.

Beltrami, H. and J. C. Mareschal. 1991. Geophysical Research Letters 18: 605-608.

Billings, W.C., J.O. Luken, D.A. Mortensen, and K.M. Peterson, 1982. Arctic tundra: A source or sink for atmospheric carbon dioxide in a changing environment? Oecologia. 52: 7-11.

Brooks, S.B., T.L. Crawford, and W.C. Oechel. 1996. Carbon dioxide emissions plumes from Prudhoe Bay, Alaska oil fields. Journal of Atmospheric Chemistry. *submitted.*

Chapin, F. S. III. 1983. Direct and indirect effects of temperature on arctic plants. Polar Biology 2: 47-52.

Crawford, T. L., R. T. McMillen and R. J. Dobosy, 1990: Development of a "generic" mobile flux platform with demonstration on a small airplane. NOAA Technical Memorandum ERL ARL-184, 81 pp.

Crawford T. L. and R. J. Dobosy, 1992: A sensitive fast-response probe to measure turbulence and heat flux from any airplane. *Boundary-Layer Meteorology* **59**, 257-278.

Dabberdt, W. F., D. H. Lenschow,T. W. Horst, P. R. Zimmerman, S. P. Oncley, and A. C. Delany, 1993: Atmosphere-surface exchange measurements. *Science* 260, 1472-1481.

Desjardins, R. L., J. I. MacPherson, P. H. Schuepp, and F. Karanja, 1989: An evaluation of aircraft flux measurements of CO_2, water vapor and sensible heat. *Boundary-Layer Meteorol.* **47**:55-69.

Dobosy, R.J., T.L. Crawford, R.T. Mcmillen and E.J. Dumas, 1996: Accurate aircraft wind measurements using the global positioning system (GPS). Proceedings of the Second International Airborne Remote Sensing Conference, San Francisco, California, June 24-27, 1996.

Eugster, W., T. Chapin, G. L. Gamarra and J. McFadden, 1996. How large are regional differences in surface heat and moisture fluxes in alaskan arctic tundra? Poster, Land-Atmosphere-Ice Interaction 1996 Science Workshop, Seattle.

Fan, S. M., S. C. Wolfsy, P. S. Bakwin, D. J. Jacob, S. M. Anderson, P. L. Kebabian, J. B. McManus, C. E. Kolb and D. R. Fitzjarrald. 1992: Micrometeorological measurements of CH_4 and CO_2 exchange between the atmosphere and subarctic tundra. Journal of Geophysical Research 97: 16,627-16644.

Flanagan, P. W., and F. L. Bunnell. 1980. Microflora activities and decomposition. Pages 291-334 *In* J. Brown, P. C. Miller, L. L. Tieszen, and F. L. Bunnell, editors. An arctic ecosystem: the coastal tundra at Barrow, Alaska. Dowden, Hutchinson, and Ross, Stroudsburg, Pennsylvania, USA.

Gold, L. W. and A. H. Lachenbruch, 1973. Thermal Conditions in Permafrost: A Review of North American Literature in Permafrost. In: "Permafrost: The North American Contribution to the Second International Conference". Yakutsk, National Academy of Sciences, Washington D.C., pp. 105-117.

Hinzman, L. D., and D. L. Kane. 1992. Potential response of an arctic watershed during a period of global warming. Journal of Geophysical Research 97: 2811-2820.

Hobbie, J. 1996, Unpublished results. The Ecosystem Center, Marine Biological Laboratory, Woods Hole, MA.

Jensen, J. R., 1983. Biophysical Remote Sensing. Annals of the Association of American Geographers. 73(1) pp. 111-132.

Kane, D., Z. Zhang, L. Hinzman and D. Goering, 1996. Frozen ground dominates hydrologic response. Poster, Land-Atmosphere-Ice Interaction 1996 Science Workshop, Seattle.

Lachenbruch, A. H., 1968. Permafrost. In: "Encyclopedia of Geomorphology", pp. 833-839, R. W. Fairbridge editor, Reinhold, Vol. III.

Lachenbruch, A. H. and B. V. Marshall. 1986 Science. 234: 689-696.

Miller, P.C., R. Kendall, and W.C. Oechel. 1983. Simulating carbon accumulation in northern ecosystems. Simulation. 40: 119-131.

Oechel, W.C. and W.D. Billings. 1992. Effects of global change on the carbon balance of arctic plants and ecosystems. *In:* T. Chapin, R. Jeffries, J. Reynolds, G. Shaver, and J. Svoboda (eds). Arctic Physiological Processes in a Changing Climate. Academic Press. pp. 139-167.

Oechel, W.C., S.J. Hastings, M. Jenkins, G. Riechers, N. Grulke, and G. Vourlitis. 1993. Recent change of arctic tundra ecosystems from a carbon sink to a source. Nature. 361: 520-526.

Oechel, W. C., W. Reeburgh, F. S. Chapin III, G. Vourlitis, and T. L. Crawford. *In press*. Large scale estimates of trace gas fluxes. Journal of Arctic Science.

Ping, C. 1996. Carbon storage in the Kuparak river basin. Poster, Land-Atmosphere-Ice Interaction 1996 Science Workshop, Seattle.

Post, W.M. 1990. Report of a workshop on climate feedbacks and the role of peat lands, tundra, and boreal ecosystems in the global carbon cycle. ORNL/TM-11457, Oak Ridge National Laboratory, Oak Ridge, TN. 32 pp.

Sedinger, J. and R. Ruess, 1996. Coastal-tundra ecosystems of the Yukon-Kuskokwim delta. Presentation and Abstract, Land-Atmosphere-Ice Interaction 1996 Science Workshop, Seattle.

Shaver, G. 1996. Species effects on biogeochemistry of tundra ecosystems, Presentation and Abstract,, Land-Atmosphere-Ice Interaction 1996 Science Workshop, Seattle.

Stull, R. B., 1988: *Boundary Layer Meteorology*. Kluwer Academic Publishers, The Netherlands. 666 pp.

Walker, D. A. 1996. A hierarchic GIS for studies of process, pattern and scale for the ARCSS flux study. Poster, Land-Atmosphere-Ice Interaction 1996 Science Workshop, Seattle.

Walker, D. A., and W. Acevedo. 1987. Vegetation and a Landsat-derived land cover map of the Beechey Point Quadrangle, Arctic Coastal Plain, Alaska. Cold Regions Research and Engineering Laboratory.

Webb, E. K., G. I. Pearman, and R. Leuning, 1980: Corrections of flux measurements for density effects due to heat and water vapor transfer. *Quart. J. R. Met. Soc,* 106: 85-100.